sustainability

MDPI

Article

Considering Carbon–Hydrogen Coupled Integrated Energy Systems: A Pathway to Sustainable Energy Transition in China Under Uncertainty

Anjie Lu [1], Jianguo Zhou [1], Minglei Qin [2] and Danchen Liu [3,*]

[1] School of Government, Nanjing University, Nanjing 210000, China; angel_nju21@163.com (A.L.); nju_jianguo@163.com (J.Z.)
[2] Nanjing Power Supply Company, State Jiangsu Electric Power Co., Ltd., Nanjing 210000, China; qml0815@163.com
[3] Nanjing Jiangbei New Area Construction and Transportation Bureau, Nanjing 210000, China
* Correspondence: liu_danchen2024@163.com

Abstract: The low-carbon construction of integrated energy systems is a crucial path to achieving dual carbon goals, with the power-generation side having the greatest potential for emissions reduction and the most direct means of reduction, which is a current research focus. However, existing studies lack the precise modeling of carbon capture devices and the cascaded utilization of hydrogen energy. Therefore, this paper establishes a carbon capture power plant model based on a comprehensive, flexible operational mode and a coupled model of a two-stage P2G (Power-to-Gas) device, exploring the "energy time-shift" characteristics of the coupled system. IGDT (Information Gap Decision Theory) is used to discuss the impact of uncertainties on the power generation side system. The results show that by promoting the consumption of clean energy and utilizing the high energy efficiency of hydrogen while reducing reliance on fossil fuels, the proposed system not only meets current energy demands but also achieves a more efficient emission reduction, laying a solid foundation for a sustainable future. By considering the impact of uncertainties, the system ensures resilience and adaptability under fluctuating renewable energy supply conditions, making a significant contribution to the field of sustainable energy transition.

Keywords: carbon capture power plant; two-stage P2G; low-carbon integrated energy system; IGDT; sustainable energy policies

check for updates

Citation: Lu, A.; Zhou, J.; Qin, M.; Liu, D. Considering Carbon–Hydrogen Coupled Integrated Energy Systems: A Pathway to Sustainable Energy Transition in China Under Uncertainty. *Sustainability* **2024**, *16*, 9256. https://doi.org/10.3390/su16219256

Academic Editor: John Bell

Received: 29 August 2024
Revised: 10 October 2024
Accepted: 16 October 2024
Published: 24 October 2024

Copyright: © 2024 by the authors. Licensee MDPI, Basel, Switzerland. This article is an open access article distributed under the terms and conditions of the Creative Commons Attribution (CC BY) license (https://creativecommons.org/licenses/by/4.0/).

1. Introduction

The world is experiencing profound transformations not seen in a century, with these changes accelerating rapidly. The increasingly severe impacts of climate change present significant challenges to global energy security [1]. In response to the critical climate issues driven by massive greenhouse gas emissions, low-carbon development has emerged as the preferred strategy for major economies to address climate change [2]. China has pledged to achieve peak carbon emissions by 2030 and attain carbon neutrality by 2060 [3].

In the decarbonization of integrated energy systems (IESs), the power generation side offers the latest advancements with the greatest potential for emission reductions. This can be categorized into the user level [4], the regional level [5], and the power generation level [6], based on the scale of power generation. On the user side, a low-carbon integrated energy system may include various small-scale, diverse energy-consuming devices such as household photovoltaic systems and energy storage solutions [7], electric vehicles [8], ground-source heat pumps, thermal storage tanks, and biogas digesters [9]. At the regional level, a low-carbon integrated energy system might consist of demand response policies targeting the user side, energy purchasing policies addressing upstream grid energy price fluctuations [10], and components like medium- and small-scale distributed photovoltaics,

wind power, diverse energy storage systems, data centers [11], power-to-hydrogen plants, and biomass cogeneration plants [12]. The generation-side low-carbon integrated energy system typically includes large-scale wind farms [13], photovoltaic power stations, carbon capture power plants [14], large power-to-hydrogen facilities [15], distribution networks, pipelines, gas storage tanks, pumped-storage power stations, and trading centers [16].

Among these, generation-side integrated energy systems are a research hotspot due to their substantial power generation capacity, high emission reduction potential, and extensive energy transmission scale. Their decarbonization pathways include carbon capture power plants [17], large-scale wind farms [18], and efficient hydropower [19], which progressively replace traditional thermal power generation methods. In this context, carbon capture power plants are particularly significant due to their deep integration with conventional thermal power generation methods [20]. They substantially decrease carbon emissions from thermal power generation, mitigating the challenges associated with large-scale wind power integration and seasonal fluctuations in hydropower [21], while retaining the inherent flexibility and adjustability of thermal power. Technically, former fossil fuel power plants can be retrofitted with carbon capture equipment to transform them into carbon capture plants. Carbon capture technologies are categorized into three types based on the CO_2 capture process: pre-combustion capture [22], oxy-fuel combustion capture [23], and post-combustion capture [24].

This paper focuses on post-combustion carbon capture, a mature technology with broad applications. Post-combustion capture refers to the process of extracting carbon dioxide (CO_2) from flue gas emissions by utilizing chemical absorbents within dedicated reactors for CO_2 separation and collection [25]. Operational modes in the capture process may include liquid storage operations, flue gas bypass operations, and comprehensive flexible operation modes that integrate both approaches [20]. The optimization of post-combustion capture equipment in conjunction with integrated energy systems is a prominent research direction in the decarbonization of source-side integrated energy systems [26]. Reference [27] studied the integration of solar thermal power plants with carbon capture devices operating in a comprehensive, flexible mode, examining the impact of varying electricity prices, power markets, and weather conditions on the system. Reference [28] proposed a novel flexible operational strategy for carbon capture technology integrated with wind power for heating purposes. This approach developed an optimization dispatch model for virtual power plants incorporating combined heat and power systems, which not only reduces carbon emissions but also increases the flexibility of both electricity and heat generation. Reference [29] investigated the integration of flexible operation carbon capture plants with pumped-storage power stations to simultaneously reduce carbon emissions and improve grid regulation capacity, particularly under conditions of deep load peaking. This strategy also contributes to reducing the overall operational costs of the system. Reference [30] designed an integrated renewable energy system that combines wind, solar, and energy storage with a carbon capture facility and coal gasification fuel cells in a highly flexible mode. A two-stage distributed robust economic dispatch model was utilized to achieve low-carbon economic dispatch objectives, addressing the high operational costs and energy consumption issues faced by carbon capture plants operating at low CO_2 concentrations.

In research on the decarbonization of power-generation-level integrated energy systems, large-scale hydrogen energy utilization is also a significant focus. After capturing CO_2 with carbon capture power plants, large-scale power-to-hydrogen equipment can convert CO_2 into H_2O and CH_4 through hydrogen generation [31,32]. Reference [33] examined an integrated energy system combining carbon capture power plants and electro-hydrogen equipment, establishing an optimal dispatch model by exploring carbon trading mechanisms and electro-thermal coupling characteristics to improve renewable energy consumption and reduce carbon emissions and operational costs. Reference [34] constructed a hydrogen-powered integrated energy system, including P2G (Power-to-Gas) equipment and carbon capture devices, addressing wind power output uncertainty and carbon trading processes with a distributed robust optimization method. Reference [34] further examined

the effects of user-side demand response, exploring the bidirectional interaction between supply-side and demand-side scheduling through the coordinated operation of combined heat and power systems, carbon capture technologies, and gas-to-power units.

However, previous studies have rarely comprehensively addressed the impact of parameter uncertainty on scheduling plans and system operations. This is especially crucial in optimizing the decarbonization of integrated energy systems, where incorporating significant levels of renewable energy sources like solar and wind power presents operational challenges for schedulers. This paper [35] introduces a hydrogen–wind–photovoltaic (HWP) system into the flexible ramping and energy markets for the first time, proposing a two-stage stochastic bi-level optimization model that accounts for the uncertainty in renewable energy output to optimize the output and revenue of HWP. Addressing the uncertainty of renewable energy output, this paper [36] constructs mathematical models for an integrated energy system (IES) and presents a multi-objective distributed robust optimization model. Using the Column and Constraint Generation algorithm and the Alternating Direction Method of Multipliers algorithm, it optimizes energy management and trading strategies for IES and electric vehicles, effectively reducing operational costs and enhancing renewable energy consumption rates. This paper [37] introduces an integrated energy hub (IEH) operational model based on Information Gap Decision Theory (IGDT) to produce green hydrogen using biomass, integrating photovoltaic and wind energy sources with hydrogen storage systems. It effectively manages uncertainties in renewable outputs, energy demands, and prices, significantly reducing operation costs and environmental impacts.

Therefore, while scholars have conducted a series of forward-looking studies on the decarbonization of power-generation-side integrated energy systems, several issues remain:

(1) The modeling of carbon capture power plants is rudimentary, and operational modes are limited, with insufficient research on the storage characteristics of carbon capture power plants under comprehensive flexible operating modes;
(2) The multi-level utilization of hydrogen energy and the carbon dioxide methanation process are not well integrated;
(3) Existing optimization scheduling relies on deterministic data, lacking research on uncertainties, particularly for renewable energy plants with high variability such as wind power and photovoltaic power.

Sustainability is at the core of modern energy system research, as nations strive to balance environmental protection with economic development. The transition to low-carbon energy systems is critical for achieving global sustainability goals, including the reduction in greenhouse gas emissions and the increase in renewable energy consumption. This research directly contributes to sustainability by optimizing the scheduling of integrated energy systems, where carbon capture and renewable energy technologies are combined to enhance both environmental and economic outcomes. Specifically, the main contributions of this work are summarized as follows:

(1) Proposing and constructing a model of carbon capture power plants based on comprehensive flexible operating modes and a two-stage electro-hydrogen equipment model, exploring the "energy time shift" characteristics of the coupled system;
(2) Using IGDT to analyze the impact of uncertainties on the power-generation-side system;
(3) Investigating carbon emissions and operating costs in deterministic scheduling models, and performing economic analysis of P2G. Additionally, the scheduling model based on IGDT, which can be divided into two strategies, is also studied.

The remainder of this paper is arranged as follows: Section 2 analyzes the comprehensive flexible operation and two-stage P2G. An economic dispatch model for low-carbon integrated energy systems on the supply side based on IGDT is introduced in Section 3. Section 4 presents the experimental results and corresponding statistical analysis. Finally, Section 5 offers a summary.

2. The Analysis of Comprehensive Flexible Operation and Two-Stage P2G

2.1. The Comprehensive Flexible Operation of Carbon Capture Power Plants

Carbon capture power plants, also known as Carbon Capture and Storage (CCS) power plants, are power stations integrated with carbon capture technology designed to effectively capture CO_2 from their emissions, thereby reducing greenhouse gas emissions. This kind of power plant typically produces energy by burning conventional fossil fuels (such as coal, natural gas, or oil) while employing advanced technologies to capture the resulting CO_2 emissions.

Gas turbine units typically operate at higher efficiencies (above 50%), but the concentration of CO_2 in the exhaust gases is relatively low (around 4–6%). The carbon capture process tends to reduce the overall efficiency of gas turbines, with energy losses typically ranging from 8% to 10%, which translates to a reduction in power output. In contrast, coal-fired steam turbine units emit CO_2 at higher concentrations (around 12–15%), making the carbon capture process more efficient. However, because coal-fired units already operate at lower efficiencies, the energy losses from carbon capture are typically in the range of 6% to 8%.

Capital costs: The capital costs of carbon capture systems on gas turbines are generally higher, ranging from USD 600 to USD 1000 per kW, whereas for coal-fired units, the costs are somewhat lower, typically between USD 500 and USD 800 per kW.

Operating costs: The operating costs for carbon capture on gas turbines are also higher, averaging around USD 40 to USD 50 per ton of CO_2. In contrast, due to the higher CO_2 concentration in coal-fired units, the operating costs are relatively lower, around USD 30 to USD 40 per ton of CO_2.

In summary, carbon capture technology is generally more economical for coal-fired steam turbine units due to their higher CO_2 concentration. However, for gas turbines, although they are more energy-efficient, the lower CO_2 concentration makes capture more costly and less economically viable. This means that gas turbine-based carbon capture would require stronger policy support, such as carbon pricing or subsidies, to improve its cost-effectiveness.

2.1.1. Energy Flow Analysis of Carbon Capture Power Plants

In this paper, carbon capture power plants utilizing post-combustion capture technology are classified according to the energy flow method into flue gas diversion type, liquid storage type, and comprehensive flexible operation type. Among these, flue gas diversion carbon capture power plants redirect a portion of the exhaust gas from combined heat and power (CHP) units to a carbon capture system, where CO_2 is extracted using a chemical absorbent, typically amine-based compounds. As illustrated in Figure 1, by adjusting the coefficient of the flue gas bypass, the quantity of CO_2 processed by the carbon capture device can be regulated, thereby adjusting the CO_2 processing energy consumption of the carbon capture device and the overall output energy consumption of the carbon capture power plant. From an energy flow perspective, the process of CO_2 flow can be understood as the flow of electrical power from CHP units. The CO_2 entering the carbon capture device represents the actual electrical power consumed; the CO_2 entering the flue gas bypass and directly emitted to the atmosphere, since it does not require processing and does not consume power from the CHP units, is effectively equivalent to the power being recycled back to the CHP units.

The liquid storage carbon capture power plant utilizes a large-scale liquid storage system to temporarily hold the absorbent used in the carbon capture process. This system consists of both a rich liquid tank and a lean liquid tank for managing the absorbent. As illustrated in Figure 1, if liquid storage tanks are considered as energy storage devices, during peak electricity usage periods, the flow into the rich liquid tank decreases, the overall electrical power of the carbon capture device decreases, and the electrical power flowing from the CHP units into the carbon capture device decreases. This can be interpreted as the liquid storage tank supplying energy to the CHP units, thereby boosting the net electrical output of the carbon capture plant. During off-peak periods, the flow into the rich liquid

tank rises, increasing the overall power consumption of the carbon capture system, along with the power transferred from the CHP units to the carbon capture facility. This can be understood as the liquid storage tank absorbing energy from the CHP units, thereby reducing the net electrical power output of the carbon capture power plant. Thus, the liquid storage type carbon capture power plant can leverage the energy storage characteristics of the liquid tanks to respond to source-side demand across different load sizes.

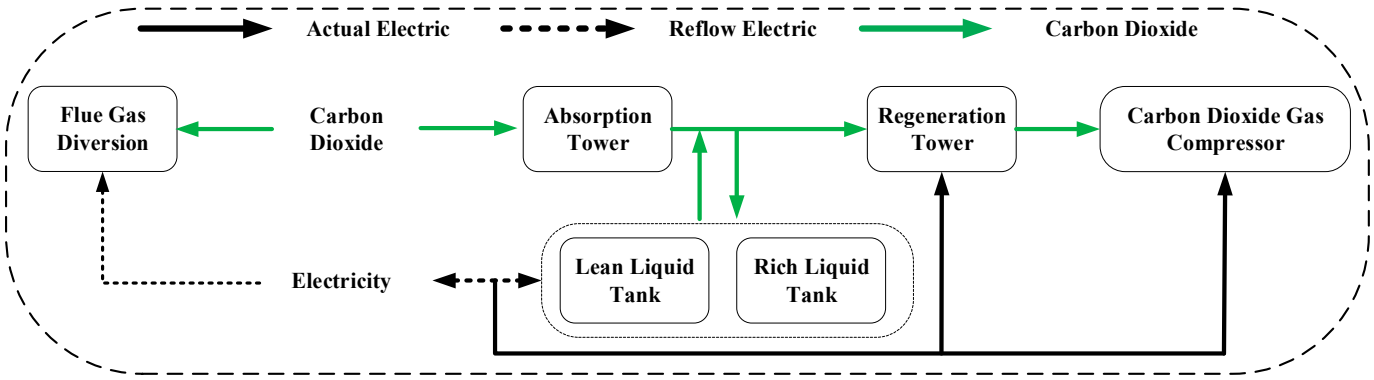


Figure 1. Liquid storage carbon capture power plant CO_2 flow diagram.

The comprehensive flexible operation of a carbon capture power plant integrates both the flue gas diversion and liquid storage operation methods. When operating in a comprehensive flexible mode, the carbon capture power plant can first divert CO_2 through a flue gas bypass before it reaches the carbon capture device and then, after CO_2 is absorbed into the liquid tanks, adjust the flow rate of the liquid tanks based on the current grid load conditions to modulate the net generation of the carbon capture power plant. Compared to the flue gas diversion and liquid storage modes, the comprehensive flexible operation carbon capture power plant offers a wider range of net power output adjustments, making it more suitable for responding to source-side output demands during significant load fluctuations. The output comparison of carbon capture power plants operating in these three modes can be seen in Figure 2.

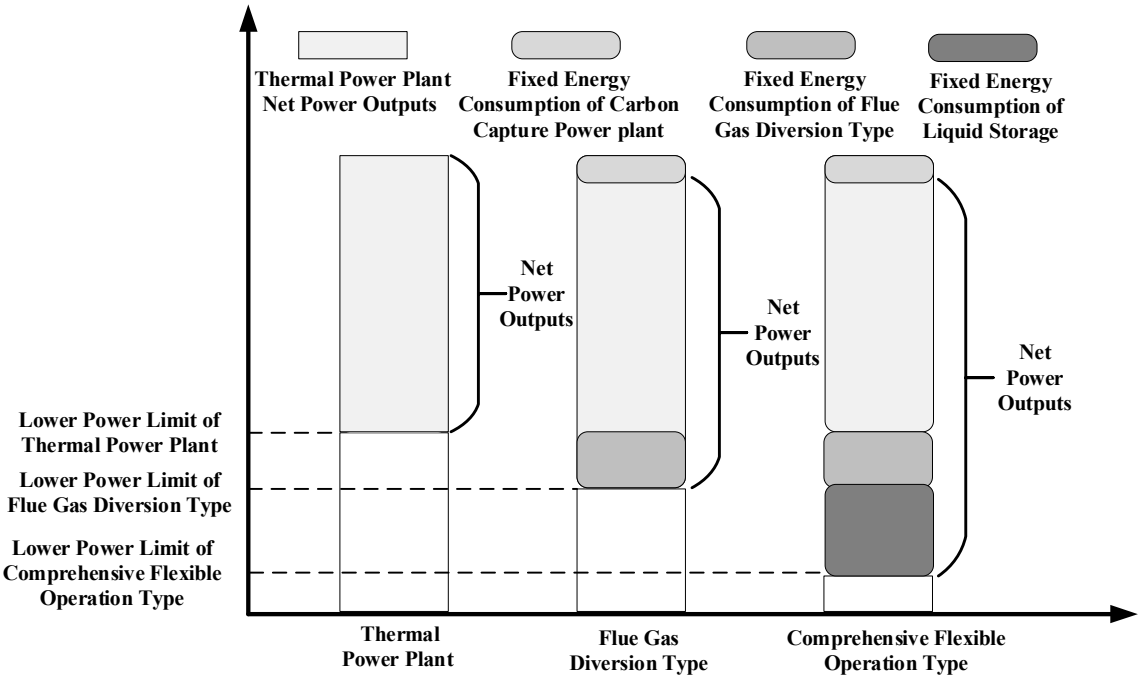


Figure 2. Comparison of net generations from carbon capture power plants.

Carbon capture power plants employing flexible operational strategies can dynamically adjust their net power output in real time to meet short-term load demands, facilitating the integration of renewable energy sources like large-scale wind power. By modulating peak and valley loads, these plants enable energy–time shifting throughout the day. During peak load periods, adjusting the flue gas bypass ratio and liquid tank storage capacity reduces the carbon capture system's power consumption, thereby increasing the net power output of the plant. The liquid tanks ensure that CO_2 emissions from CHP units are efficiently absorbed during high-demand times, helping to lower overall CO_2 emissions. Conversely, during off-peak periods, the carbon capture system's power usage is increased to process the CO_2 solution stored in the liquid tanks from the peak periods, reducing the plant's net power output and supporting wind energy consumption during low-demand times. As illustrated in Figure 3, this comprehensive flexible operational approach enables effective energy time-shifting, enhancing the efficiency of CHP units by reducing start–stop cycles, minimizing energy losses during start-up and shutdown processes, improving overall energy efficiency, reducing maintenance costs, and prolonging equipment lifespan.

Carbon capture systems typically consist of large absorption towers, regeneration towers, and supporting equipment such as pipelines, pumps, and compressors. These components have significant physical dimensions and weight, which impose stringent space requirements on the facility. Existing gas–steam combined cycle plants were not originally designed with dedicated space for carbon capture systems, especially those built in earlier years. Therefore, during retrofitting, factors such as layout space, piping connections, and system integration must be carefully analyzed. In most cases, the retrofit requires the optimization and rearrangement of existing equipment. For instance, some non-essential facilities, such as storage tanks and non-critical pipelines, may need to be relocated to free up space for carbon capture installations.

A notable example is the Huaneng Green Energy Power Plant carbon capture project in Hebei, China, which became operational in 2020. During the retrofit, the project carefully considered equipment dimensions and spatial limitations. By reconfiguring auxiliary equipment and adjusting the flue gas discharge path, the installation of the carbon capture system was successfully completed.

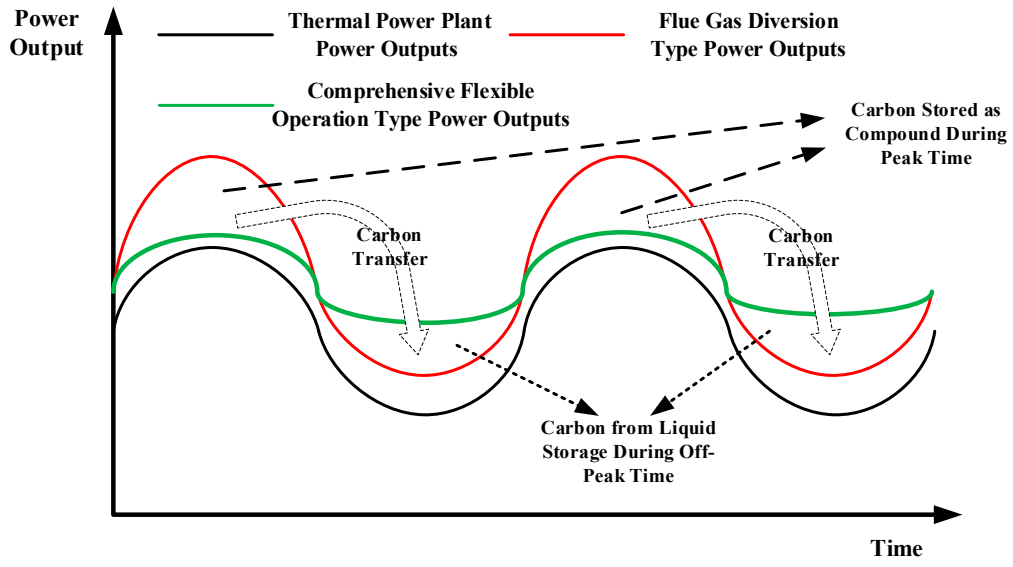


Figure 3. Energy time shifting in carbon capture power plants.

In contrast, for newly built carbon capture units, space is often reserved at the design stage. For example, in the China Resources Power Datong Project in Guangdong, sufficient space was allocated for the future installation of carbon capture equipment during the initial design phase, and the flue gas treatment process was optimized to facilitate smooth installation later on.

2.1.2. Mathematical Model of Carbon Capture Power Plants

Based on Figure 1, a mathematical model for carbon capture power plants operating under a comprehensive flexible mode is established. In this mode of operation, the total amount of CO_2 processed by the carbon capture equipment includes two parts: the quantity of CO_2 absorbed in the absorption tower after being diverted through the flue gas bypass, and the quantity of CO_2 stored in the rich liquid tank pending flow into the regeneration tower for processing and separation.

$$E_{all,t} = E_{pool,t} + \beta\zeta E_{ccs,t} \tag{1}$$

$$0 \le \zeta \le 1 \tag{2}$$

$$0 \le E_{all,t} \le a\beta b_{ccs} P_{ccs,\max} \tag{3}$$

where $E_{all,t}$ represents the total quantity of CO_2 that the carbon capture equipment can process at the *t-th* period; $E_{pool,t}$ represents the quantity of CO_2 in the rich liquid storage tank awaiting processing in the regeneration tower at the *t-th* period; β is the capture efficiency of the carbon capture equipment; ζ is the flue gas diversion ratio after introducing the flue gas bypass system to the carbon capture equipment; $E_{ccs,t}$ is the total quantity of CO_2 produced by the CHP units at *t-th* period; a is the maximum operating state factor of the absorption and regeneration towers in the carbon capture equipment; b_{ccs} is the CO_2 emission intensity of the CHP units; $P_{ccs,max}$ is the minimum production electric power of the carbon capture power plant.

The operation of the carbon capture system involves both fixed and variable energy consumption, with the latter comprising compression, regeneration, and absorption energy consumption. However, since the energy required for absorption is relatively minor compared to the other components, it is typically disregarded. As a result, the variable energy consumption of the carbon capture system primarily consists of compression and regeneration energy consumption, in addition to the fixed energy usage. Therefore, the total power demand of the carbon capture plant can be defined as the sum of the fixed energy consumption, the operational energy consumption, and the net energy production of the facility.

$$P_{ccs,t} = P_{j,t} + P_{f,t} + P_{op,t} \tag{4}$$

$$P_{op,t} = \eta E_{all,t} \tag{5}$$

$$E_{ccs,t} = b_{ccs} P_{ccs,t} \tag{6}$$

where $P_{ccs,t}$ is the production electric output of the power plant combining CHP and carbon capture equipment at *t-th* period; $P_{j,t}$ is the net production electric power of the power plant combining CHP and carbon capture equipment at the *t-th* period; $P_{f,t}$ is the fixed energy consumption of the carbon capture equipment during operation at the *t-th* period; $P_{op,t}$ is the energy usage during the operation of the carbon capture equipment at the *t-th* period; and η is the power coefficient required per unit of CO_2 processed.

$$P_{f,t} \le P_{op,t} + P_{f,t} \le a\beta b_{ccs}\eta\zeta_{\max} P_{ccs,\max} + P_{f,t} \tag{7}$$

where ζ_{max} is the flue gas diversion ratio after introducing the flue gas bypass system to the carbon capture equipment. When the ratio is 1, it means that the flue gas bypass system is not being used.

By substituting Equation (6) into Equation (7), we can derive the range of the net production power of the carbon capture power plant in operation under a comprehensive flexible mode as follows:

$$P_{ccs,\min} - a\beta b_{ccs}\eta\zeta_{\max} P_{ccs,\max} - P_{f,t} \le P_{j,t} \le P_{ccs,\max} - P_{f,t} \tag{8}$$

where $P_{ccs,min}$ represents the minimum production electric power of the carbon capture power plant.

If we consider the operation mode as solely flue gas bypass without a liquid storage tank carbon capture power plant, where the maximum operational state factor for both the absorption and regeneration towers is set to 1, and there is no rich liquid tank between the regeneration tower and absorption tower to set input and production flow conditions, the extent of the net production power of the carbon capture power plant can be derived as follows:

$$P_{ccs,\min} - \beta b_{ccs} \eta \zeta_{\max} P_{ccs,\max} - P_{f,t} \le P_{j,t} \le P_{ccs,\max} - P_{f,t} \tag{9}$$

If we consider the operation mode as solely liquid storage tank without a flue gas bypass carbon capture power plant, meaning that the CO_2 emissions from the CHP units cannot be flexibly adjusted through the flue gas bypass ratio, which, according to relevant literature, is typically set at 0.7, the range of the net production power of the carbon capture power plant can be determined as follows:

$$P_{ccs,\min} - 0.7\beta b_{ccs} \eta P_{ccs,\max} - P_{f,t} \le P_{j,t} \le P_{ccs,\max} - P_{f,t} \tag{10}$$

Figure 2 presents a comparison of the net power generation from carbon capture power plants across three distinct operational modes. The figure clearly shows that plants utilizing a comprehensive flexible mode exhibit a broader range of net power generation scenarios. With the same CHP thermal reserve requirements, these plants achieve lower net power output, making them more effective in absorbing large-scale wind energy during periods of low electricity demand.

The liquid storage tank serves as the key component enabling the comprehensive flexible operation of carbon capture power plants. By incorporating rich and lean liquid tanks, the plant can shift high carbon emissions from peak load periods to lower emissions during off-peak times, while also enhancing the integration of wind power during low-demand periods. The corresponding mathematical model is as follows:

$$P_{j,t} = P_{ccs,t} - P_{f,t} - \eta(E_{pool,t} + \beta\zeta b_{ccs} P_{ccs,t}) \tag{11}$$

$$P_{j,t} = (1 - \eta\beta\zeta b_{ccs}) P_{ccs,t} - P_{f,t} - \eta E_{pool,t} \tag{12}$$

First, modeling the rich liquid storage tank involves defining the inflow and outflow rates of the rich liquid storage tank as follows:

$$E_{pool,t} = f_{out,t} \tag{13}$$

$$f_{in,t} = \zeta\beta b_{ccs} P_{ccs,t} \tag{14}$$

where $f_{out,t}$ represents the quantity of CO_2 flowing out from the rich liquid storage tank to the regeneration tower for desorption at the *t-th* period; $f_{in,t}$ denotes the quantity of CO_2 flowing into the rich liquid storage tank awaiting desorption at the *t-th* period.

Next, the calculation for the quantity of CO_2 absorbed by the regeneration tower and the absorption tower is as follows:

$$E^{in}_{all,t} = \zeta b_{ccs} P_{ccs,t} \tag{15}$$

$$E_{reform,t} = f_{in,t} + f_{out,t} \tag{16}$$

where $E^{in}{}_{all,t}$ represents the quantity of CO_2 flowing into the regeneration tower for absorption at the *t-th* period and $E_{reform,t}$ denotes the total quantity of CO_2 flowing into the regeneration tower for desorption at the *t-th* period.

Finally, the volume of CO_2 solution stored in the liquid tank can be determined from the mole calculation of the chemical reaction equation as follows:

$$V_{pool,t} = \frac{E_{pool,t} M_{MEA}}{M_{CO_2} E_{reform,t} \rho_r C_r} \tag{17}$$

where $V_{pool,t}$ represents the volume of the CO_2 solution in the storage tank at the *t-th* period; M_{MEA} is the molar quantity of the MEA (Monoethanolamine) solution; M_{CO2} is the molar quantity of CO_2; ρ_r is the density of the MEA solution; C_r is the concentration of the MEA solution.

2.2. Two-Stage P2G

2.2.1. Two-Stage P2G Energy Analysis

P2G technology is a method that uses electrical energy to decompose water (H_2O) into hydrogen (H_2) and oxygen (O_2), typically through a process known as electrolysis. This represents a clean method of producing hydrogen. Considering the characteristics of P2G and the industrial application of hydrogen, this paper proposes a two-stage treatment for P2G devices, encompassing the processes of electrolysis for hydrogen production and the subsequent conversion of hydrogen into natural gas. Unlike traditional single-stage P2G models that are merely based on conversion efficiency, the two-stage electrolytic hydrogen model utilizes a stepped utilization of hydrogen energy. Through the methanation process of hydrogen, where CO_2 is absorbed to produce methane, thereby reducing carbon emissions, the process is detailed as shown in Figure 4. During the electrolysis process, the electrolyzer (EL) converts water into hydrogen and oxygen using the input electrical energy; this paper focuses solely on the subsequent utilization of hydrogen. For the utilization of hydrogen, a methanation reactor (MR), hydrogen fuel cells (HFCs), and hydrogen storage tanks (HSTs) are set up. The methanation reactor can produce methane from hydrogen and carbon dioxide via the chemical reaction equation $CO_2 + 4H_2 == CH_4 + 2H_2O$. Hydrogen fuel cells can generate electricity and heat from the combustion of hydrogen. Hydrogen storage tanks can store or supply hydrogen in real time for system use. By refining the P2G devices through a two-stage model and studying the stepped utilization of hydrogen, and considering that the combustion efficiency of hydrogen is higher than that of methane, and hydrogen fuel cells can directly transform hydrogen energy into both electricity and heat—unlike the traditional process, which converts hydrogen into methane before using CHP units for electricity and heat—this approach eliminates the energy transmission process and enhances energy utilization efficiency. This has significant implications for integrating P2G devices into comprehensive energy systems to achieve overall system energy saving and emission reduction.

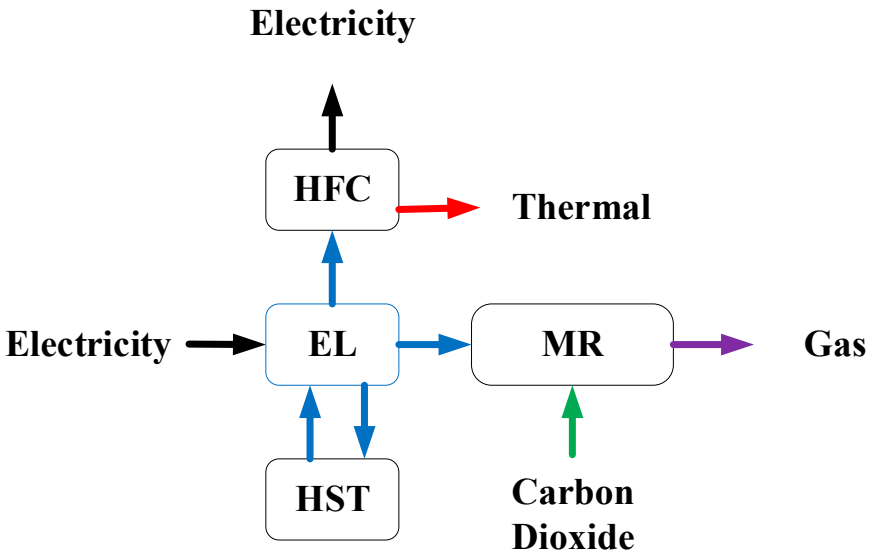


Figure 4. Two-stage energy bus diagram for Power-to-Gas.

The efficiency of the methanation process typically depends on the type of reactor and the operating conditions. Modern fixed-bed methanation reactors have demonstrated CO_2 conversion rates of around 90% in both laboratory settings and industrial demonstrations,

with the purity of the synthesized methane usually exceeding 95%. The overall system efficiency of methanation is influenced by the capture, compression, reaction, and post-treatment stages. Conventional energy utilization efficiency ranges from 45% to 60%, and if renewable energy sources such as wind or solar power are used for hydrogen production via water electrolysis, the overall efficiency tends to be even lower.

Methanation has been applied in several large-scale projects, such as Germany's Audi e-gas plant and France's Jupiter 1000 project. This technology typically employs the Sabatier reaction to combine CO_2 with renewable hydrogen to produce methane, which is compatible with existing natural gas infrastructure. The Jupiter 1000 project in France showcases the deep integration of methanation with power grids, supporting grid flexibility. The project achieved methanation efficiency of approximately 85%.

2.2.2. Two-Stage P2G Mathematical Model

Compared to previous modeling approaches for P2G devices, the two-stage P2G model pays more attention to modeling the constituent parts of P2G equipment. As illustrated in Figure 4, a two-stage P2G device can include components such as an electrolyzer, a methanation reactor, a hydrogen fuel cell, and a hydrogen storage tank.

(a) Overall Mathematical Model for P2G
This includes the total electricity consumption of the P2G equipment, which is specifically the distinction between the electrical power supplied by the hydrogen fuel cell and the electrical power absorbed by the electrolyzer, and the overall rate of natural gas supply, which is the production rate of the methanation reactor.

$$P^{e}_{p2g,t} = P^{e}_{hfc,t} - P^{in}_{el,t} \tag{18}$$

$$V_{p2g,t} = V^{CH_4}_{mr,t} \tag{19}$$

where ${P^{e}}_{p2g,t}$ represents the production electrical power of the electrolytic hydrogen production device at the *t-th* period; ${P^{H2}}_{el,t}$ is the hydrogen power produced by the electrolyzer at the *t-th* period; ${P^{e}}_{hfc,t}$ is the production electrical power of the hydrogen fuel cell at the *t-th* period; ${V^{CH4}}_{mr,t}$ is the volume of methane produced by the methanation reactor at the *t-th* period; and $V_{p2g,t}$ is the volume of natural gas provided by the electrolytic hydrogen production device at the *t-th* period.

(b) Electrolyzer Model

$$P^{H_2}_{el,t} = \eta_{el} P^{in}_{el,t} \tag{20}$$

$$P^{in}_{el,\min} \le P^{in}_{el,t} \le P^{in}_{el,\max} \tag{21}$$

$$\Delta P^{in}_{el,\min} \le P^{in}_{el,t} - P^{in}_{el,t-1} \le \Delta P^{in}_{el,\max} \tag{22}$$

where η_{el} represents the electrolytic efficiency of hydrogen production by the electrolyzer; ${P^{in}}_{el,t}$ is the electrical input to the electrolyzer at the *t-th* period; ${P^{in}}_{el,min}$ is the minimum electrical power input to the electrolyzer; ${P^{in}}_{el,max}$ is the maximum electrical power input to the electrolyzer; $\Delta {P^{in}}_{el,min}$ is the minimum ramping power for the electrolyzer over a unit time interval; ${P^{in}}_{el,t-1}$ is the electrical power input to the electrolyzer at the $t-1th$ period; $\Delta {P^{in}}_{el,max}$ is the maximum ramping power for the electrolyzer over a unit time interval.

(c) Methanation Reactor Model

$$P^{CH_4}_{mr,t} = \eta_{mr} P^{H_2}_{mr,t} \tag{23}$$

$$V^{CH_4}_{mr,t} = \frac{P^{CH_4}_{mr,t}}{q_{CH_4}} \tag{24}$$

$$P^{H_2}_{mr,\min} \le P^{H_2}_{mr,t} \le P^{H_2}_{mr,\max} \tag{25}$$

$$\Delta P^{H_2}_{mr,\min} \le P^{H_2}_{mr,t} - P^{H_2}_{mr,t-1} \le \Delta P^{H_2}_{mr,\max} \tag{26}$$

$$E^{CO_2}_{mr,t} = \rho_{CO_2} V^{CO_2}_{mr,t} = \rho_{CO_2} V^{CH_4}_{mr,t} \tag{27}$$

where $P^{CH4}{}_{mr,t}$ is the methane power produced by the methanation reactor at the *t-th* period; η_{mr} is the efficiency of methane production by the methanation reactor; $P^{H2}{}_{mr,t}$ is the hydrogen power input to the methanation reactor at the *t-th* period; q_{ch4} is the combustion power per unit volume of methane; $P^{H2}{}_{mr,min}$ is the minimum hydrogen power input to the methanation reactor; $P^{H2}{}_{mr,max}$ is the maximum hydrogen power input to the methanation reactor; $\Delta P^{H2}{}_{mr,min}$ is the minimum ramping power input to the methanation reactor over a unit time interval; $P^{H2}{}_{mr,t-1}$ is the hydrogen power input to the methanation reactor at the $t-1th$ period; $\Delta P^{H2}{}_{mr,max}$ is the maximum ramping power input to the methanation reactor over a unit time interval; $E^{CO2}{}_{mr,t}$ is the quantity of CO_2 input to the methanation reactor at the *t-th* period; ρ_{co2} is the standard density of CO_2 at a specified temperature and atmospheric pressure; and $V^{CO2}{}_{mr,t}$ is the volume of CO_2 input to the methanation reactor at *t-th* period.

(d) Hydrogen Fuel Cell

$$P^{e}_{hfc,t} = \eta^{e}_{hfc,t} P^{H_2}_{hfc,t} \tag{28}$$

$$P^{h}_{hfc,t} = \eta^{h}_{hfc,t} P^{H_2}_{hfc,t} \tag{29}$$

$$Q^{H_2}_{p2g,t} = P^{h}_{hfc,t} \tag{30}$$

$$P^{H_2}_{hfc,\min} \le P^{H_2}_{hfc,t} \le P^{H_2}_{hfc,\max} \tag{31}$$

$$\Delta P^{H_2}_{hfc,\min} \le P^{H_2}_{hfc,t} - P^{H_2}_{hfc,t-1} \le \Delta P^{H_2}_{hfc,\max} \tag{32}$$

$$\gamma_{hfc,\min} \le \frac{P^{h}_{hfc,t}}{P^{e}_{hfc,t}} \le \gamma_{hfc,\max} \tag{33}$$

where $\eta^{e}{}_{hfc,t}$ is the hydrogen-to-electricity conversion efficiency of the hydrogen fuel cell at the *t-th* period; $P^{H2}{}_{hfc,t}$ is the input power to the hydrogen fuel cell at the *t-th* period; $P^{h}{}_{hfc,t}$ is the heat generation of the hydrogen fuel cell at the *t-th* period; $\eta^{h}{}_{hfc,t}$ is the hydrogen-to-heat conversion efficiency of the hydrogen fuel cell at the *t-th* period; $Q^{H2}{}_{p2g,t}$ is the thermal power production of the electrolytic hydrogen production device at the *t-th* period; $P^{H2}{}_{hfc,min}$ is the minimum input power to the hydrogen fuel cell; $P^{H2}{}_{hfc,max}$ is the maximum input power to the hydrogen fuel cell; $\Delta P^{H2}{}_{hfc,min}$ is the minimum ramping power of the hydrogen fuel cell over a unit time interval; $\Delta P^{H2}{}_{hfc,max}$ is the maximum ramping power of the hydrogen fuel cell over a unit time interval; $P^{H2}{}_{hfc,t-1}$ is the input power to the hydrogen fuel cell at the $t-1th$ period; $\gamma_{hfc,min}$ is the minimum thermal–electric efficiency of the hydrogen fuel cell; and $\gamma_{hfc,max}$ is the maximum thermal–electric efficiency of the hydrogen fuel cell.

2.3. Joint Operation of Carbon Capture Power Plants and P2G Based on Storage Characteristics

Conventional energy storage systems typically profit by leveraging load or price variations. For instance, electrical storage systems discharge electricity during peak demand to reduce load stress and capitalize on lower costs during off-peak times by storing power. The net power generation characteristics of carbon capture power plants operating in a comprehensive flexible mode have already been discussed. During peak demand, carbon capture desorption power is decreased, functioning similarly to releasing energy from a storage system, thereby boosting the plant's net power output. Conversely, during off-peak

times, desorption power is increased, akin to energy absorption by the storage system, which lowers the plant's net power output.

This paper combines two-stage P2G devices to propose a novel carbon-capture–P2G coupled system. The core idea is to utilize the storage tank to temporarily store the CO_2 produced during peak electricity demand periods and then release it during off-peak periods for use in methanation processes within the P2G system. This approach significantly reduces the dependence of P2G on external carbon sources, lowers the operational costs of P2G, and enhances the efficiency of the entire system. More importantly, this method enables more efficient use of captured CO_2, reducing storage costs and effectively avoiding environmental risks associated with storage leaks. In the context of electrical energy storage, during off-peak periods, the carbon capture power plant increases the desorption power of the carbon capture system, lowering the plant's net power output, effectively making the system act as if it were absorbing electricity. Meanwhile, the P2G system is activated, utilizing the electrolyzer to produce hydrogen, which can be used in methanation reactors, hydrogen fuel cells, and other applications, thereby supporting large-scale wind power utilization. During peak demand, the carbon capture plant decreases desorption power, raising the net power output, similar to releasing stored electricity. For carbon energy storage, during off-peak times, the plant desorbs significant amounts of CO_2, with the P2G system producing methane via the methanation reactor, promoting carbon consumption across the system. During peak demand, CO_2 emissions from CHP units are stored in tanks, facilitating carbon storage throughout the system.

The integration of P2G technology with carbon capture power plants operating in a comprehensive flexible mode enables an efficient system of carbon cycling and dynamic carbon utilization. This mode not only optimizes carbon resource management but also enhances the system's capacity to integrate renewable energy, especially wind power. In this process, P2G technology plays a crucial role, converting excess wind power into hydrogen or methane, thereby providing an effective pathway for energy storage and conversion. Simultaneously, carbon capture power plants, by operating flexibly within this system, adjust their electricity generation to meet changing grid demands while efficiently capturing and utilizing stored CO_2. This joint-operation mode not only ensures the system's low-carbon performance but also considers the overall economic benefits of the system while enhancing wind power integration capacity. This innovative approach better balances power supply and demand, reduces wind power curtailment, and achieves carbon emission reduction, offering an effective pathway towards energy transition and low-carbon development goals. The implementation of this model demonstrates the potential for sustainable development within energy systems and provides new insights and directions for future energy technology development.

3. Economic Optimization Model Based on IGDT

3.1. Overall System Operational Framework

By coupling the carbon capture power plant, working under a comprehensive flexible mode, with a two-stage P2G system and integrating it into a typical comprehensive energy system, we form the overall operational framework depicted in Figure 5. Within the system, energy flows can be categorized into five forms: electricity, heat, gas, carbon, and hydrogen. Electricity bus devices, including wind power, photovoltaics, electrical energy storage, and the main grid, collectively supply energy to meet the system's electrical load and the energy needs of electric heat pumps. Furthermore, CHP units can supply electricity after accounting for the energy consumed by the carbon capture system. The two-stage P2G system utilizes electricity through the electrolyzer while generating power via hydrogen fuel cells. In terms of heat, gas turbines, electric heat pumps, and hydrogen fuel cells within the P2G system provide thermal energy to meet the system's heat load requirements. For natural gas, the system can obtain it from the main gas grid or through the P2G system's methanation reactor to support the CHP units and gas load needs. The carbon dioxide energy balance is primarily managed between the CHP units and the carbon capture system,

with the P2G system's methanation reactor consuming CO_2 captured by the carbon capture device. Hydrogen energy balance is handled within the two-stage P2G system, where the electrolyzer produces hydrogen through water electrolysis, and hydrogen fuel cells generate electricity and heat from hydrogen. Any surplus hydrogen can be stored in tanks for future system use.

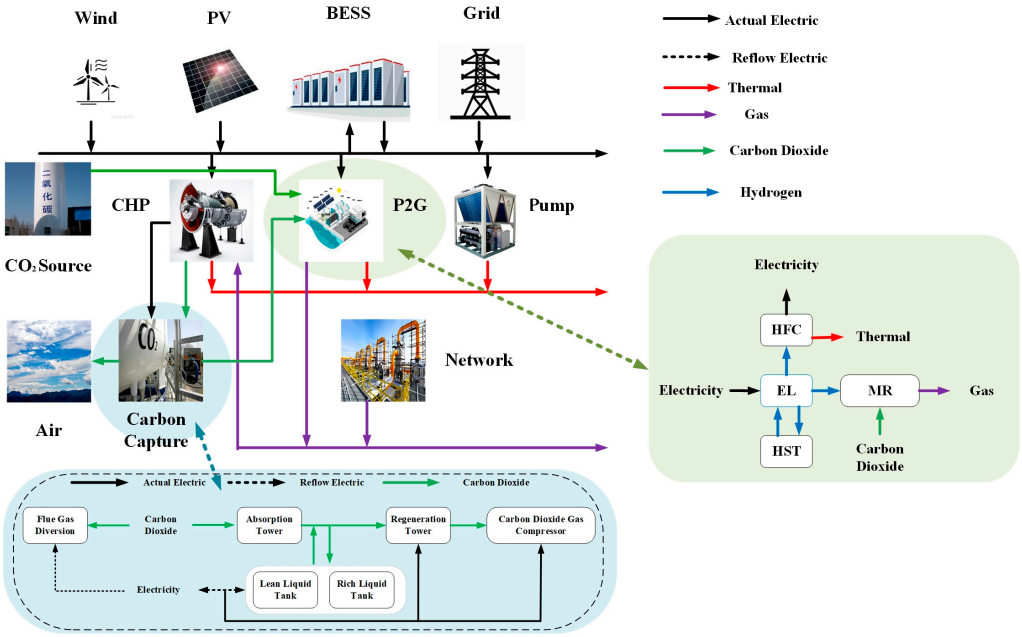


Figure 5. Dispatch structure of the system.

3.2. Deterministic Objective Function

In China, the primary objective of the power grid is to ensure the security and stability of electricity supply, rather than solely focusing on economic efficiency. One key value of carbon capture power plants is their ability to consume large amounts of renewable energy, such as wind power, which helps mitigate the issue of wind curtailment. Additionally, these plants possess real-time peak-shaving capabilities, providing extra power support during grid peak load periods. Compared to economic considerations, the stability and security of electricity supply take precedence in China's power system. Therefore, in this study, the investment and retrofit costs of carbon capture power plants have not been considered.

The goal of this paper is to minimize the operating costs of the low-carbon integrated energy system depicted in Figure 5. As such, the objective function consists of six sub-cost components: startup and shutdown costs of CHP units, penalties for wind curtailment, operational and maintenance expenses related to carbon trading and sequestration, operational and maintenance costs for electrolytic hydrogen production equipment, costs for externally purchased energy, and the operational and maintenance expenses for carbon capture equipment.

$$C_{total} = C_{chp} + C_w + C_t + C_{p2g} + C_{pur} + C_{ccs} \tag{34}$$

where C_{total} represents the total operating cost of the system; C_{chp} is the startup and shutdown costs of CHP units; C_w is the system's wind curtailment penalty costs; C_t is the operational and maintenance costs of carbon trading and carbon sequestration; C_{p2g} is the operational and maintenance costs of electrolytic hydrogen production equipment; C_{pur} is the cost of energy purchased externally for the system; and C_{ccs} is the working and maintenance costs of carbon capture equipment.

In the dispatchable mode, CCHP systems or coal-fired power plants often require frequent start-ups and shut-downs or operate at partial loads, which can significantly

reduce their operational efficiency. When load fluctuations are large, the thermal efficiency of the equipment decreases, leading to greater energy losses.

Partial load operation: The combustion efficiency and heat utilization rate decrease, resulting in lower overall energy efficiency. Studies have shown that coal-fired power plants can experience efficiency losses of 5% to 10% when operating at partial loads.

Frequent start-ups and shut-downs: In dispatchable mode, coal-fired combined cycle units may undergo frequent cycling, increasing mechanical wear and fuel consumption, further reducing their efficiency.

Moreover, the fuel heat utilization rate is significantly reduced in dispatchable mode, especially when the equipment operates under unstable load conditions. Coal-fired units are more efficient at higher loads, where they can better utilize the thermal energy of the fuel. However, at lower loads, incomplete combustion and increased heat loss cause the fuel heat utilization rate to drop, further diminishing the economic viability of the equipment under dispatchable conditions.

However, this paper focuses on the scheduling possibilities of integrating carbon capture systems and power-to-hydrogen equipment in coal-fired plants. The study aims to propose a novel energy system, with data nodes set at one-hour intervals, thus avoiding the need for frequent cycling over short periods. Therefore, the efficiency reduction typically seen in CCHP systems or coal-fired units operating in dispatchable mode is not considered in this context.

(a) Startup and Shutdown Costs of CHP Units:

$$\begin{aligned} C_{chp} &= \sum_{t=1}^{24} k_t (a_5 {P_{chp,t}}^2 + b_5 P_{chp,t} + c_5) \\ &+ \sum_{t=1}^{24} k_t (1 - k_t) q_{chp,t} \end{aligned} \tag{35}$$

where k_t is a binary variable at the *t-th* period, taking values of 0 or 1, representing the operational status of CHP units at the *t-th* period. A value of 0 means the CHP unit is shutdown, and a value of 1 means the CHP unit is operating; a_5, b_5, and c_5 are cost parameters per unit of power when the CHP units are operating; and $q_{chp,t}$ is the cost coefficient when CHP units are shutdown at the *t-th* period.

(b) Wind Curtailment Penalty Costs:

$$C_w = \sum_{t=1}^{24} w_q (P_{wind,t}^{pre} - P_{wind,t}) \tag{36}$$

where W_q is the penalty coefficient per unit of power for curtailed wind power; ${P^{pre}}_{wind,t}$ is the day-ahead forecasted wind power generation.

(c) Operational and Maintenance Costs of Carbon Trading and Carbon Sequestration:

$$C_t = C_{CO_2} + C_y \tag{37}$$

where C_{CO2} is the cost of carbon trading under current policies and C_y is the cost required for carbon sequestration of CO_2 under current policies.

$$C_{CO_2} = price_{CO_2} (E_{ccs,t} - \sum_{t=1}^{24} D_{chp,t}) \tag{38}$$

where $price_{CO2}$ is the carbon trading price; $E_{ccs,t}$ represents the total CO_2 emissions from CHP units at the *t-th* period and $D_{chp,t}$ is the regulated carbon emission allowance for CHP units under current policies at the *t-th* period.

$$D_{chp,t} = \gamma_{chp} P_{chp,t} \tag{39}$$

where γ_{chp} is the carbon emission quota coefficient per unit of power for CHP units after combustion under current policies.

$$C_y = \varepsilon E_{fold,t} \tag{40}$$

where ε is the cost coefficient per unit quantity of CO_2 for sequestration using carbon capture equipment and $E_{fold,t}$ is the total CO_2 sequestered by carbon capture equipment at the *t-th* period.

(d) Operational and Maintenance Costs of Electrolytic Hydrogen Production Equipment:

$$C_{p2g} = \sum_{t=1}^{24} \kappa_{CO_2} E_{buy,t} + \sum_{t=1}^{24} \kappa_{p2g} P_{p2g,t} \tag{41}$$

where K_{CO2} is the unit raw material cost for the unit to purchase CO_2 from the outside and K_{p2g} is the unit power operational and maintenance cost for electrolytic hydrogen production equipment.

(e) The Cost of Energy Purchased Externally by the System:

$$C_{pur} = \sum_{t=1}^{24} price_{e,t} P_{grid,t} + \sum_{t=1}^{24} \kappa_{CO_2} price_{g,t} (V_{net,t} + V_{chp,t}) \tag{42}$$

where $price_{e,t}$ is the real-time electricity price at the *t-th* period, with time-of-use electricity pricing being utilized in this paper; $price_{g,t}$ is the natural gas price at the *t-th* period; and $V_{chp,t}$ is the volume of natural gas consumed by CHP units at the *t-th* period.

(f) Working and Maintenance Costs of Carbon Capture Equipment:

$$C_{ccs} = \frac{C_{flow}(1+\theta)^{n_{flow}}\theta}{365[(1+\theta)^{n_{flow}} - 1]} + \frac{C_{\tan k} V_{\tan k}(1+\theta)^{n_{\tan k}}\theta}{365[(1+\theta)^{n_{\tan k}} - 1]} \tag{43}$$

where C_{flow} is the total construction cost of carbon capture equipment using flue gas bypass method; θ is the annual depreciation rate percentage for carbon capture equipment; n_{flow} is the service life of carbon capture equipment using the flue gas bypass method; C_{tank} is the total construction cost for carbon capture equipment using the liquid storage tank method; and n_{tank} is the service life of carbon capture equipment using the liquid storage tank method.

The cost of CCS is relatively high, particularly in terms of the investment and operating costs for new equipment. To promote the adoption of CCS technology in China, the government and relevant institutions have employed various strategies to provide financial support for CCS projects and drive the widespread application of these technologies through policy initiatives. The funding sources for CCS projects can be broadly categorized into government fiscal support, investments from state-owned enterprises, and international financial assistance. Additionally, China has gradually established a national carbon emissions trading market, which offers funding opportunities for CCS through carbon trading. Companies can generate revenue by reducing carbon emissions, earning carbon credits, and selling them on the market. As a result, the construction costs of CCS equipment are not considered in this study.

3.3. Carbon Capture Power Plant Dispatch Model Based on IGDT

The comprehensive flexible carbon capture power plant constructed in this paper optimizes scheduling based on certain results of system load (wind and photovoltaic production, multi-energy user demand). However, considering that in the real market, it is impossible to accurately predict the production of new energies such as wind and photovoltaic, nor to determine the energy demand of day-ahead users, there is always the potential for economic losses due to unforeseen events. Therefore, this paper proposes a method based on IGDT (Information Gap Decision Theory) to address the uncertainties of wind, light, and load [38]. Unlike traditional stochastic planning problems, IGDT treats all uncertainties as a collection of a single uncertainty factor [34], describing the probabilistic

characteristics of this uncertainty through models such as the envelope model, ellipsoidal model, and fractional uncertainty model [38]. It also sets expected cost or profit indicators, allowing the optimization to consider both the energy costs and the robustness of the system compared to traditional methods.

Referencing [38] and considering the energy characteristics of the carbon capture power plant with P2G included, this paper employs the fractional uncertainty model to describe load uncertainty:

$$F(\chi, \overline{\kappa}_t) = \{\kappa_t : |\kappa_t - \overline{\kappa}_t| \geq \chi \overline{\kappa}_t\}, \chi \geq 0 \tag{44}$$

where χ represents the fluctuation range of load demand; κ_t is the real-time load value at the *t-th* period; and $\overline{\kappa}_t$ is the forecasted load value at the *t-th* period.

From Equation (43), it can be deduced that the upper limit of the system load demand, considering uncertainty factors, is $(1+\chi)\overline{\kappa}_t$, and the lower limit can be expressed as $(1-\chi)\overline{\kappa}_t$. When χ equals 0, it represents accurate load forecasting, which corresponds to the system optimization model without considering load uncertainty. Considering the profit-seeking nature of the user system, this paper divides the uncertain model optimization scheduling into a risk-seeking model and a risk-averse model.

3.3.1. IGDT Optimization Scheduling Based on the Risk-Seeking Model

The system based on the risk-seeking model adopts an optimistic attitude towards the uncertainties and fluctuations, believing that these uncertainties will bring more economic benefits to the system. Therefore, when establishing related scheduling strategies, minimizing the fluctuation range of the system is set as the upper-level objective. Additionally, ensuring the system cost under the uncertain model is lower than the system cost under the original certain model is set as the optimization lower-level objective to achieve greater economic benefits. Thus, the IGDT optimization scheduling model based on the risk-seeking model is represented as follows:

$$\begin{cases} obj \min \chi \\ s.t. \begin{cases} \min C_{total} \leq C_{total}^{ZQ} = C_{total}^{0}(1-\varepsilon_m) \\ \kappa_t \in F(\chi, \kappa_t) \\ Equations\ (48)–(67) \end{cases} \end{cases} \tag{45}$$

where ${C_{total}}^{ZQ}$ represents the cost threshold of the system based on a risk-seeking approach and ε_m represents the opportunity deviation factor, ranging from [0, 1). A smaller value of the factor indicates a lower degree of risk-seeking by the system, and ${C_{total}}^{0}$ represents the operating cost of the system under a deterministic objective function.

The analysis reveals that for a source-side low-carbon integrated energy system based on the joint operation of carbon capture power plants and P2G, the smaller the fluctuation range of uncertainty for photovoltaic, wind, and load, that is, the smaller the lower-level constraints of the system, the more it can utilize a risk-seeking strategy to enhance the system's multi-energy coupling and thus reduce costs and gain more benefits. Therefore, the lower-level optimization objective in the original model can be simplified to the maximum operating cost being less than or equal to the system operating cost when the load fluctuation reaches its lower limit. The original bi-level optimization model can be simplified to a single-level optimization model.

$$\begin{cases} obj \min \chi \\ s.t. \begin{cases} C_{total} \leq C_{total}^{ZQ} = C_{total}^{0}(1-\varepsilon_m) \\ \kappa_t = \overline{\kappa}_t(1-\chi) \\ Equations\ (48)–(67) \end{cases} \end{cases} \tag{46}$$

3.3.2. IGDT Optimization Scheduling Based on the Risk-Averse Model

The IGDT optimization scheduling model based on the risk-averse approach is more cautious during system operation, considering that the uncertainty of wind, solar, and load will lead to increased operating costs. Thus, the system considers the maximum uncertainty fluctuation as the upper optimization objective, that is, aiming for greater system robustness, while also meeting the constraint of system operating costs under the robustness level factor. Therefore, the IGDT optimization scheduling model based on the risk-averse approach is represented as follows:

$$\begin{cases} obj \max \chi \\ s.t. \begin{cases} \max C_{total} \le C_{total}^{GB} = C_{total}^{0}(1+\delta_m) \\ \kappa_t \in F(\chi, \kappa_t) \\ Equations\ (48)–(67) \end{cases} \end{cases} \tag{47}$$

where $C_{total}{}^{GB}$ represents the cost threshold of the system based on a risk-averse approach and δ_m represents the robustness level factor, ranging from [0, 1). A larger value indicates a higher degree of risk aversion by the system and stronger robustness.

Similarly, analysis reveals that when the fluctuation degree of the load in the lower-level objective function is maximized, the lower-level objective function reaches its maximum value. Therefore, the original bi-level optimization model can be simplified to a single-level optimization model.

$$\begin{cases} obj \max \chi \\ s.t. \begin{cases} C_{total} \le C_{total}^{GB} = C_{total}^{0}(1+\delta_m) \\ \kappa_t = \overline{\kappa}_t(1+\chi) \\ Equations\ (48)–(67) \end{cases} \end{cases} \tag{48}$$

3.4. Balance Equations and Constraint Conditions

This paper constructs an integrated energy system based on Figure 5, which can be categorized into five types of energy sources: electricity, thermal energy, natural gas, carbon dioxide, and hydrogen.

(a) Electric Energy Balance Bus:

$$P_{wind,t} + P_{pv,t} + P_{grid,t} + P_{j,t} + P_{p2g,t}^{e} + P_{bess,t}^{dis} - P_{bess,t}^{ch} - P_{eb,t} = L_{e,t} \tag{49}$$

where $P_{wind,t}$ represents the wind output at the *t-th* period; $P_{pv,t}$ is the pv output integrated into the system at the *t-th* period; $P_{grid,t}$ is the electrical power purchased from the main grid at the *t-th* period; $P^{e}{}_{p2g,t}$ is the electrical power provided by the electrolytic hydrogen production device at the *t-th* period; $P^{dis}{}_{bess,t}$ is the discharge power of the electrical energy storage equipment at the *t-th* period; $P^{ch}{}_{bess,t}$ is the charging power of the electrical energy storage equipment at the *t-th* period; $P_{eb,t}$ is the power consumption of the heat pump units at the *t-th* period; and $L_{e,t}$ is the electrical load of the system at the *t-th* period.

(b) Thermal Energy Balance Bus:

$$Q_{chp,t}^{h} + Q_{p2g,t}^{h} + Q_{eb,t} = L_{h,t} \tag{50}$$

where $Q^{h}{}_{chp,t}$ is the thermal power provided by the CHP units at the *t-th* period; $Q^{h}{}_{p2g,t}$ is the thermal power provided by the electrolytic hydrogen production device at the *t-th* period; $Q_{eb,t}$ is the thermal power provided by the heat pump units at the *t-th* period; and $L_{h,t}$ is the thermal load of the system at the *t-th* period.

(c) Natural Gas Balance Bus:

$$V_{net,t} + V_{p2g,t} - V_{chp,t} = L_{g,t} \tag{51}$$

where $V_{net,t}$ is the volume of natural gas obtained from the gas network at the *t-th* period and $L_{g,t}$ is the gas load of the system at the *t-th* period.

(d) Carbon Dioxide Balance Bus:

$$E_{mr,t}^{CO_2} = E_{buy,t} + E_{p2g,t} \tag{52}$$

where $E_{buy,t}$ is the total volume of CO_2 purchased externally by the electrolytic hydrogen production device at the *t-th* period and $E_{p2g,t}$ is the total volume of CO_2 obtained from the carbon capture device by the electrolytic hydrogen production device at the *t-th* period.

$$\begin{aligned} E_{fold,t} &= f_{in,t} + f_{out,t} - E_{mr,t}^{CO_2} \\ &= \zeta\beta b_{ccs} P_{ccs,t} + E_{pool,t} - E_{mr,t}^{CO_2} \end{aligned} \tag{53}$$

where $E_{fold,t}$ is the total volume of CO_2 sequestered by the carbon capture device at the *t-th* period.

(e) Hydrogen Gas Balance Bus

$$P_{el,t}^{H_2} = P_{mr,t}^{CH_4} + P_{hfc,t}^{H_2} + P_{esc,t}^{H_2} - P_{esd,t}^{H_2} \tag{54}$$

where $P^{H2}{}_{esc,t}$ represents the stored power in the hydrogen storage device within the electrolytic hydrogen production device at the *t-th* period and $P^{H2}{}_{esd,t}$ is the released power from the hydrogen storage device within the electrolytic hydrogen production device at the *t-th* period.

Equipment constraints may include CHP unit ramping and production constraints, heat pump unit production constraints, conventional equipment production constraints, and energy storage device constraints,

(a) CHP Unit Constraints

$$\max\left\{P_{chp,\min}^{e} - C_{r1}P_{chp,t}^{h}, C_m(P_{chp,t}^{h} - P_{h0})\right\} \le P_{chp,t}^{e} \le P_{chp,\max}^{e} - C_{r2}P_{chp,t}^{h} \tag{55}$$

where C_{r1} is the electric–thermal conversion coefficient when the CHP unit's electrical power production is at its minimum; C_m is the linear supply slope of the thermal power and electrical power of the CHP unit; P_{h0} is the thermal power production when the CHP unit's electrical power production is at its minimum; and C_{r2} is the electric–thermal conversion coefficient when the CHP unit's electrical power production is at its maximum.

$$P_{ccs,t} = P_{chp,t} \tag{56}$$

$$P_{chp,t}^{e} = P_{j,t} \tag{57}$$

$$Q_{chp,t}^{h} = P_{chp,t}\eta_{chp}^{h} \tag{58}$$

$$\left|P_{chp,t} - P_{chp,t-1}\right| \le ramp \tag{59}$$

where $P_{chp,t-1}$ represents the production power of the CHP unit at the $t-1th$ period and *ramp* is the maximum ramping constraint of the CHP unit between adjacent time periods.

$$V_{chp,t} = a_2 + b_2 P_{chp,t} + c_2 (P_{chp,t})^2 \tag{60}$$

where a_2, b_2, and c_2 are the gas consumption parameters when the CHP unit is operational.

(b) Production Constraint of Heat Pump Units

$$Q_{eb,t} = \eta_{eb} P_{eb,t} \tag{61}$$

where $Q_{eb,t}$ is the thermal power production of the heat pump unit at the *t-th* period and η_{eb} is the electricity-to-heat efficiency of the heat pump unit.

(c) Production Constraint for Conventional Equipment:

$$P_{\min} \leq P_t \leq P_{\max} \tag{62}$$

(d) Energy Storage Device Constraints:

$$0 \leq P_{dis,t} \leq P_{dis,\max} \tag{63}$$

where $P_{dis,t}$ is the discharge power of the energy storage device at *t-th* period and $P_{dis,max}$ is the maximum discharge power of the energy storage device at *t-th* period.

$$0 \leq P_{ch,t} \leq P_{ch,\max} \tag{64}$$

where $P_{ch,t}$ is the charging power of the energy storage device at *t-th* period and $P_{ch,max}$ is the maximum charging power of the energy storage device at *t-th* period.

$$0 \leq Z_t \leq Z_{\max} \tag{65}$$

where Z_t is the energy storage status of the energy storage device at the *t-th* period and Z_{max} is the maximum capacity of the energy storage device.

$$Z_t = Z_{t-1} + P_{es,t} \tag{66}$$

where Z_{t-1} is the energy storage status of the energy storage device at the $t-1th$ period and $P_{es,t}$ is the final production power of the energy storage device at the *t-th* period.

$$u_{dis}(t) + u_{ch}(t) = 1 \tag{67}$$

where $u_{dis}(t)$ is a binary variable, taking values of 0 or 1, indicating the discharge flag of the energy storage device and $u_{ch}(t)$ is a binary variable, taking values of 0 or 1, indicating the charging flag of the energy storage device.

$$u_{dis}(t) + u_{ch}(t) = 1 \tag{68}$$

4. Case Stuides

4.1. Basic Configurations

Using the scenario depicted in Figure 5 as a case study, this paper performs an example analysis for a typical winter day in a specific location to validate the economic advantages and the carbon emission reductions offered by the proposed low-carbon integrated energy system on the power generation side. In the case study, the CHP units operate with three units in parallel, where the largest capacity CHP unit is modified to connect to a comprehensive flexible-operation carbon capture device. Figure 6 shows the day-ahead forecast for user load and new energy output load, Table 1 lists the local electricity prices, and the local natural gas price is 0.35 RMB/(kWh). Parameters for the CHP units are provided in Table 2. Energy conversion parameters, carbon capture power-plant-related parameters, and two-stage P2G device parameters can be found in reference [39], while actual carbon emission model parameters are in reference [40]. The unit carbon trading price is 0.268 RMB/kg, and the cost of wind curtailment penalties is uniformly 0.2 RMB/(kWh).

The data used in this study are from the winter season in Ningxia, China, where photovoltaic (PV) power generation is predominantly distributed and geographically dispersed. Although PV power generation can achieve high efficiency with ample sunlight in winter, the region's cold temperatures and frequent fog reduce the consistency of PV output. Moreover, in Ningxia's large-scale renewable energy projects, the installed capacity of wind power significantly surpasses that of PV. Therefore, this study primarily focuses on the integration of large-scale wind farms, emphasizing the impact of wind power output uncertainty on system dispatch.

The wind power output is generated by multiple wind farms located in Ningxia, China, which are coordinated through the grid for joint dispatch. Ningxia has several large wind farms, and through unified grid management, they can collectively provide

more stable, high-level power generation during certain periods. This geographical distribution advantage allows the wind farms in different areas to complement one another, enabling more continuous power generation when wind conditions are favorable through coordinated operation.

The morning peak in electricity load during winter is not solely driven by residential demand but is significantly influenced by industrial activities. Ningxia, being an industrial hub, is home to numerous energy-intensive enterprises. The increased electricity demand for industrial production in winter leads to a sharp rise in electrical load during the morning hours.

The peak in thermal load data observed in the morning is primarily due to the concentrated demand for heat from industrial users, especially in areas related to factory and industrial operations. The heating systems in Ningxia predominantly serve the production needs of industrial facilities rather than residential heating. Therefore, the morning thermal load peak is closely linked to the heat demand of factories in the region.

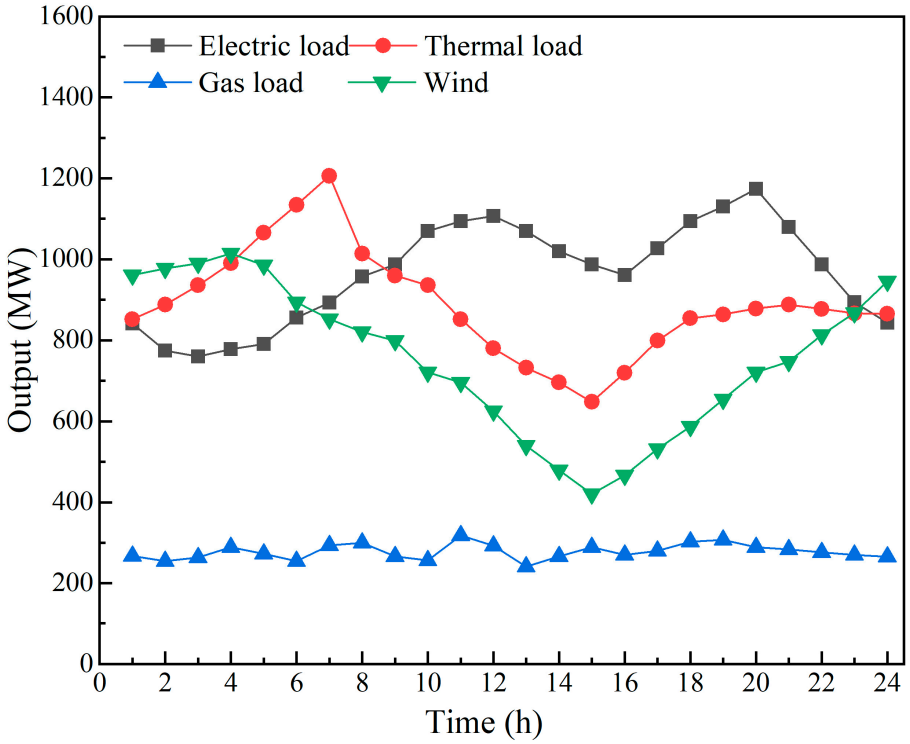


Figure 6. Day-ahead forecast load in case studies.

Table 1. Time-of-use electricity price.

	Periods	RMB/kWh
Off-Peak.	1:00–6:00, 23:00–24:00	0.5
Normal	7:00–8:00, 13:00–17:00	0.73
Peak	9:00–12:00, 18:00–22:00	1.21

Table 2. CHP units parameters.

Num.	Limits (MW)	Ramp (MW/h)	Fuel Cost Coefficient
G1	550/160	60	0.0014/200/750
G2	200/40	25	0.0023/100/600
G3	200/40	15	0.0015/250/400

4.2. Scenario Analysis of the Deterministic Scheduling Model

Firstly, a day-ahead optimization model for the low-carbon integrated energy system is developed under specific wind and solar load conditions, with three scenarios designed for comparison:

Scenario 1: Only the original low-carbon integrated energy system and electrolytic hydrogen production are considered, without the inclusion of a carbon capture device.

Scenario 2: The system integrates a flue gas bypass carbon capture device along with a two-stage electrolytic hydrogen production system.

Scenario 3: A comprehensive flexible-mode carbon capture device and a two-stage electrolytic hydrogen production system are integrated into the low-carbon energy system.

The comparison outcomes for these three scenarios are presented in Table 3.

Table 3. Cost results under three scenarios.

	Scenario 1	Scenario 2	Scenario 3
Gas Purchase Cost/Ten Thousand Yuan	90.11	85.91	81.11
Coal Cost for Thermal Power/Ten Thousand Yuan	70.59	9.78	82.91
Carbon Trading Cost/Ten Thousand Yuan	19.81	−10.33	−12.58
Operating Cost/Ten Thousand Yuan	20.27	229	26.58
Wind Curtailment Cost/Ten Thousand Yuan	6.6	5.41	2.51
Wind Power Absorption Rate	91.47%	912%	98.23%
Total Cost/Ten Thousand Yuan	201.73	192.98	180.52
Total Carbon Emissions/t	4817.59	3300.09	2855.01

(1) Comparative Analysis between Scenario 1 and Scenario 2

Comparing the results in Table 3, it is evident that, compared to Scenario 1, Scenario 2 introduces a flue gas bypass carbon capture device into the operating system. From the perspective of total carbon emissions, the bypass carbon capture device reduces carbon emissions by 31.5% and, on the basis of improving wind power consumption rate by 2.65%, reduces the total system cost by 5%. Additionally, because the two-stage electrolytic hydrogen production device includes a methanation reactor, the system can transfer CO_2 captured in the bypass carbon capture to the methanation reactor for methanation, producing methane. This process reduces the storage and transportation costs of CO_2 within the system to a certain extent and significantly lowers carbon trading costs, and Scenario 2 can trade surplus carbon emission allowances. Profits from these trades also help reduce the overall system costs. However, with the inclusion of the flue gas bypass, the net generation of the carbon capture power plant must be reduced by the operational power of the bypass system, resulting in a 19.2% increase in operating costs in Scenario 2 compared to Scenario 1. Despite this, the incorporation of the bypass carbon capture device lowers the overall system costs and carbon emissions while also enhancing the utilization of wind power.

(2) Comparative Analysis between Scenario 2 and Scenario 3

In Scenario 3, a liquid storage tank system is added to the bypass-style carbon capture device from Scenario 2. As shown in Table 3, this results in a 13.5% decrease in total carbon emissions, a 6.25% reduction in system costs, a 21.78% drop in carbon trading expenses, and an 11% increase in wind power utilization compared to Scenario 2. The analysis suggests that the liquid storage tank enhances the flexibility of the carbon capture device's net power output and strengthens its "energy time-shift" capability. By adjusting the input and output flow parameters, it regulates CO_2 intake, enabling better load adjustment during peak and valley periods. This reduces overall system emissions, boosts profits from selling carbon credits, and lowers carbon trading costs.

Figures 7 and 8 illustrate the output of the carbon capture power plant and the conventional thermal units for Scenarios 2 and 3, respectively. In Figure 7, during peak load periods, the net generation of the carbon capture plant operating in a comprehensive

flexible mode exceeds that of the bypass-style system. In these periods, the storage tank fully absorbs CO_2, deferring processing to off-peak times. This reduces the operational load of the carbon capture system and increases the plant's net power generation. During off-peak periods, the comprehensive flexible carbon capture plant ramps up CO_2 processing to handle the emissions captured during peak periods, which decreases its net power output. Meanwhile, wind power generation in the system peaks and the reduced net generation from the carbon capture plant allow for greater wind energy consumption. In Figure 8, it is evident that Scenario 3 significantly reduces the output of conventional thermal power units, even achieving zero output during off-peak periods. This highlights the superior "energy time-shift" capability and enhanced CO_2 processing performance of the carbon capture plant operating in a comprehensive flexible mode.

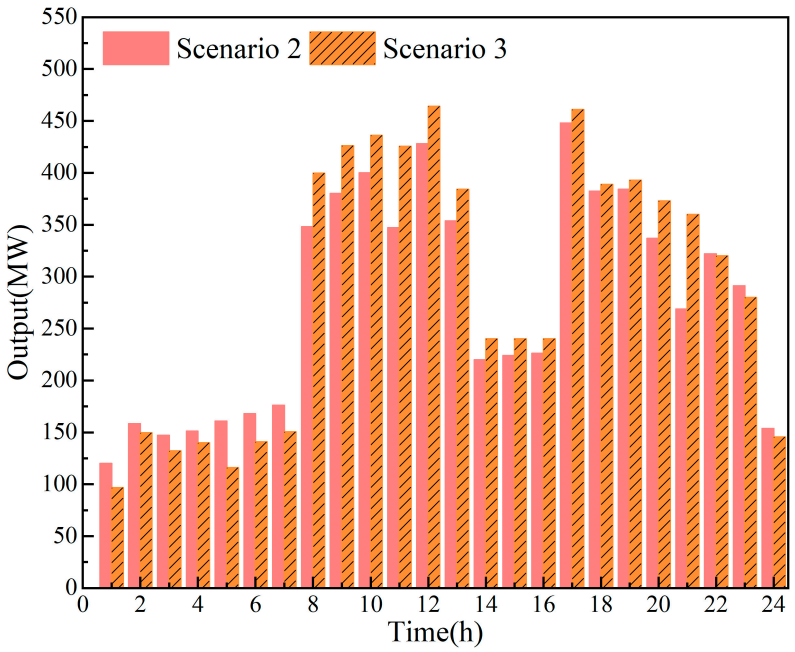


Figure 7. Carbon capture power plant outputs.

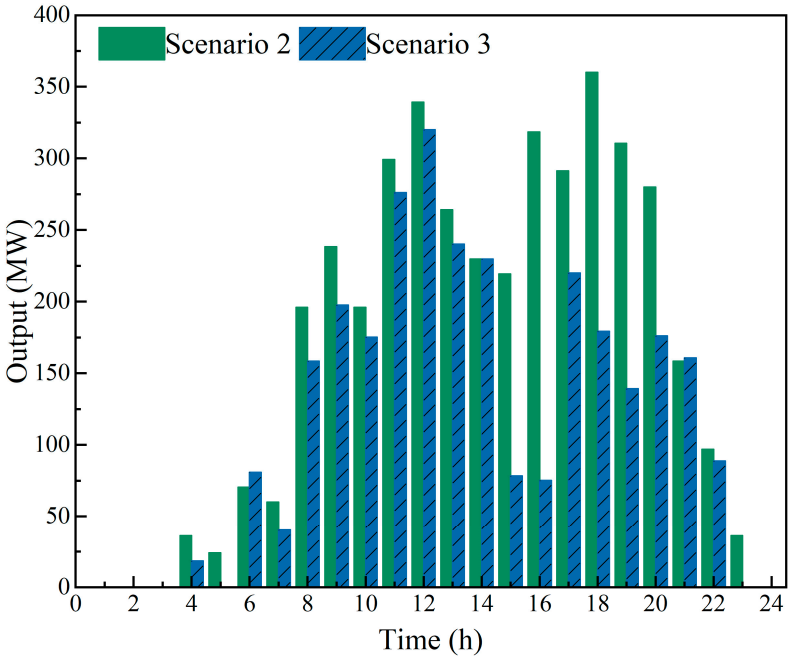


Figure 8. Outputs of other conventional thermal power units.

Figure 9 illustrates the electricity power composition in Scenario 3. Analysis shows that during off-peak periods, the system's electrical power is primarily supplied by conventional units and wind power. At this time, the carbon capture power plant essentially does not generate power but instead processes CO_2 absorbed during peak periods and provides reactants for the methanation reactor. In terms of electricity consumption, electrolyzers operate to produce hydrogen, supplying raw materials to the methanation reactor while further enhancing the consumption capacity for wind power. During peak load periods, as the wind power output decreases, the output of the carbon capture power plant increases. At this time, electrical energy storage and hydrogen fuel cells work to smooth out the differences between peak and off-peak electricity demand. This demonstrates that the addition of two-stage electrolytic hydrogen production equipment enriches the energy options of the low-carbon integrated energy system on the power generation side. It can better couple with the "energy time shift" characteristic of the carbon capture power plant, providing more choices for hydrogen utilization and CO_2 processing and storage.

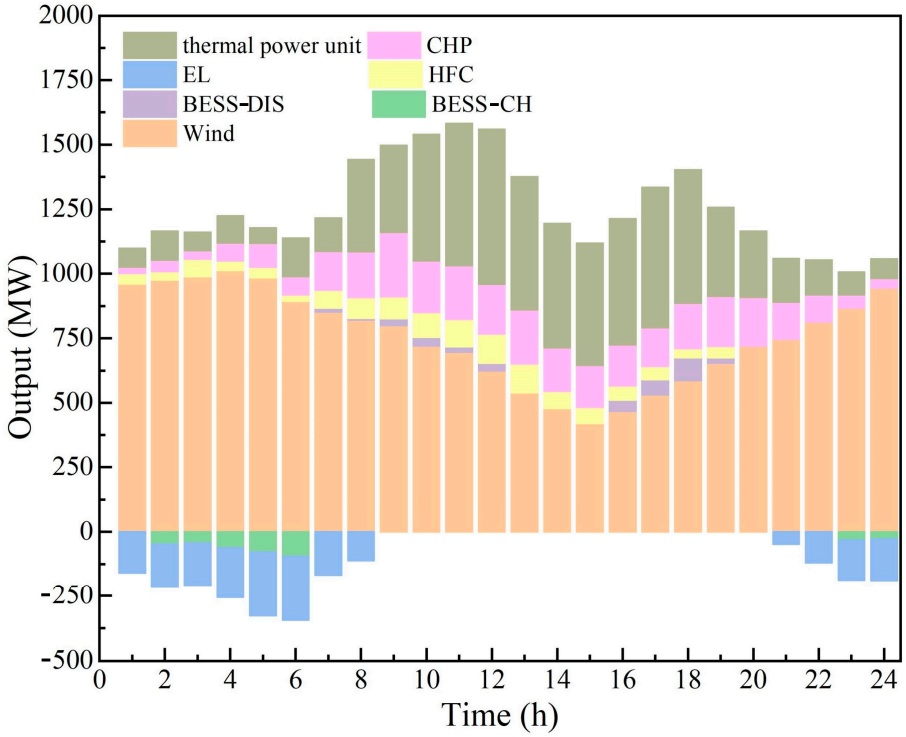


Figure 9. Scenario 3: composition of electrical power.

4.3. Analysis of Carbon Emissions in the Deterministic Scheduling Model

This paper examines the energy-saving and emission-reduction capabilities of a low-carbon integrated energy system on the power generation side. As shown in Table 3, both bypass-style and comprehensive flexible carbon capture devices significantly cut the system's carbon emissions by 31.25% and 40.52%, respectively, while also increasing wind power consumption rates by 2.65% and 6.76%. These findings underscore the critical role carbon capture devices play in reducing emissions and saving energy in low-carbon power generation systems. A comparison between Scenarios 2 and 3 highlights the necessity of incorporating a liquid storage tank into the carbon capture system. The tank's "time-shifting" feature allows CO_2 to be absorbed during peak load times without immediate processing, thereby improving the net generation of the carbon capture plant and reducing the output from the other CHP units. This, in turn, lowers overall system emissions. During off-peak periods, the system processes the stored CO_2, decreasing the net generation of the carbon capture plant and supporting greater wind power utilization, further cutting emissions. In summary, integrating a carbon capture device in comprehensive flexible

mode provides multiple advantages for a low-carbon energy system. It not only reduces total carbon emissions and enhances wind power consumption but also contributes to energy efficiency and emission reduction across various dimensions.

4.4. Economic Analysis of P2G in the Deterministic Scheduling Model

The two-stage electrolytic hydrogen production is an additional consideration in this paper, compared to traditional electrolytic hydrogen production coupled with carbon capture systems. To demonstrate the advantages of two-stage electrolytic hydrogen production, three operational scenarios are set up as follows.

Scenario 4: The original low-carbon integrated energy system on the power generation side, which does not include a P2G device but includes a carbon capture device operating in a comprehensive flexible mode.

Scenario 5: The original low-carbon integrated energy system on the power generation side, including a traditional single-stage P2G device and a carbon capture device operating in a comprehensive flexible mode.

Scenario 6: The original low-carbon integrated energy system on the power generation side, including a two-stage P2G device (electrolyzer, methanation reactor, hydrogen fuel cell, and hydrogen storage tank) and a carbon capture device operating in a comprehensive flexible mode.

Table 4 displays the scheduling results under three different P2G device configurations. The analysis reveals that P2G devices can reduce the system's carbon emissions, carbon trading costs, and total operating costs while improving the overall energy efficiency of the system. Particularly in Scenario 6, after implementing a two-stage treatment for the P2G device, compared to Scenarios 4 and 5, carbon emissions were reduced by 27.46% and 20.76%, respectively, and energy efficiency was improved by 1.68% and 1.1%, respectively. The primary reason is that the hydrogen fuel cells in the two-stage P2G device have a higher energy utilization efficiency for electricity and heat, avoiding the need to convert thermal energy from electrical energy, thus reducing energy transmission losses and enhancing system energy efficiency. The methanation reactor in the two-stage device provides a production pathway for converting system CO_2 into methane, reducing the costs of carbon transportation and storage. Through the methanation process, carbon is directly converted into fossil fuel, thereby reducing the system's total and carbon trading costs while decreasing the system's need for externally purchased gas. This enhances the system's energy independence and lowers the total carbon emissions. Hence, refining P2G devices offers multiple advantages for low-carbon integrated energy systems on the power generation side.

Table 4. Dispatch results of P2G under three scenarios.

	Scenario 4	**Scenario 5**	**Scenario 6**
Total Carbon Emissions/t	3936.49	3603.31	2855.01
Carbon Trading Cost/Ten Thousand Yuan	15.94	2.84	−12.58
Gas Purchase Cost/Ten Thousand Yuan	97.71	86.01	81.11
Wind Curtailment Cost/Ten Thousand Yuan	10.38	7.94	2.51
Total Cost/Ten Thousand Yuan	226.14	198.32	180.52
Energy Efficiency/%	955	95.13	96.23

4.5. Analysis of the Addition of PV Power Generation

The research in this paper focuses on regions similar to Ningxia in China, which are typically characterized by their inland location, distance from the ocean, vast land area, sparse population, and abundant wind and solar resources. Consequently, this paper selects wind power as the primary source of renewable energy, coupling it with carbon capture systems and power-to-hydrogen devices to explore the optimal dispatch of a low-carbon integrated energy system under multi-energy coupling. In the primary case analysis of the article, solar photovoltaic (PV) power was not directly considered for integration. While

PV power is indeed an important renewable energy source in the northwest regions of China, such as Ningxia, it typically generates higher output around noon, when electricity demand is also higher. Furthermore, PV installations tend to be more distributed in scale compared to large-scale wind farms. The primary issue with PV power is not large-scale integration and consumption, as is the case with wind power.

Therefore, in the case analysis and system construction presented in this paper, PV power was not included. If PV power were to be integrated into the system studied in this paper, its role would primarily reduce the cost of purchasing electricity from the external grid and decrease the output of thermal power plants, which would also partially reduce the system's overall carbon emissions. However, it has little direct relevance to the wind, carbon capture plants, and hydrogen–methane production chain discussed in this paper. Nevertheless, since PV power occupies a substantial proportion on the generation side, this paper considers the integration of day-ahead PV power forecast output in Section 4.5. The PV power plant used in this study is located in northern Ningxia, and the actual measured data from a PV power plant with an installed capacity of 200 MW are shown in Figure 10. The plant is integrated into the system operation architecture depicted in Figure 5, operating under the dispatch mode of Scenario 3. The optimized operational results obtained are presented in Table 5. Specific photovoltaic parameters can be found in the reference [19].

Table 5. Cost results under PV scenarios.

	Scenario 3	Scenario 3 + PV
Gas Purchase Cost/Ten Thousand Yuan	81.11	74.84
Carbon Trading Cost/Ten Thousand Yuan	−12.58	−12.62
Operating Cost/Ten Thousand Yuan	26.58	28.74
Wind Curtailment Cost/Ten Thousand Yuan	2.51	3.34
Wind Power Absorption Rate	98.23%	97.45%
Total Cost/Ten Thousand Yuan	180.52	174.94
Total Carbon Emissions/t	2855.01	2788.47

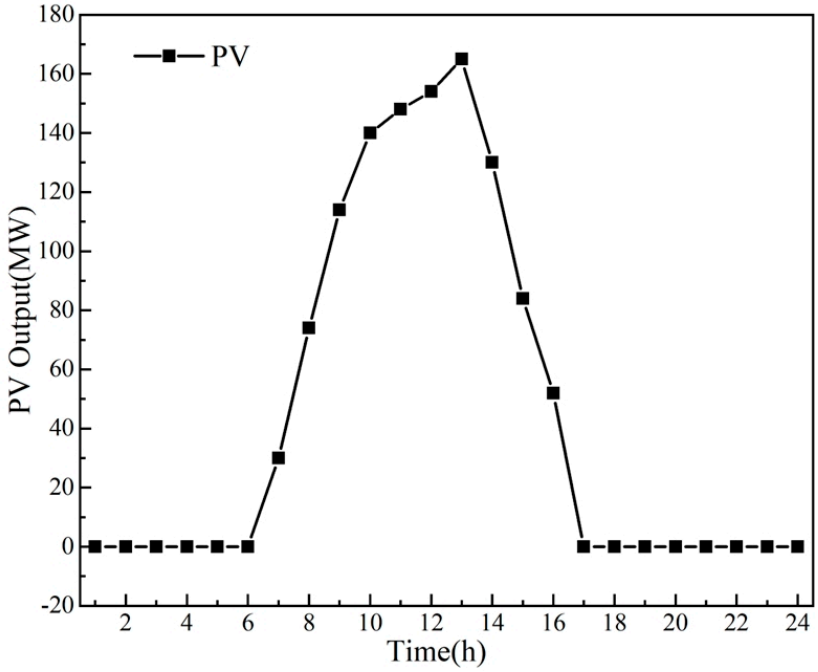


Figure 10. Output power of the PV Unit.

Table 5 presents the optimization results of Scenario 3 before and after the integration of PV power. It can be observed that with the addition of PV output, the system's gas

purchase costs are reduced. While the operating costs increase due to the inclusion of PV maintenance costs, the overall costs decrease due to a reduction in thermal power generation. In terms of carbon emissions, the introduction of PV power significantly reduces the overall emissions. However, the wind power utilization rate slightly decreases. Upon analysis, this is due to the fact that the introduction of PV power reduces the need for thermal generation during peak demand periods, leading to a decrease in the amount of CO_2 stored in the liquid storage tanks. Consequently, during nighttime, when wind power output is high, the total CO_2 available for processing in the carbon capture plant decreases, slightly reducing the wind power utilization rate.

From this analysis, it is clear that PV power can reduce both the overall carbon emissions and the operating costs of the system. However, in practical operation, PV power plays a relatively disconnected role from the wind power, carbon capture plants, and hydrogen utilization chain. PV power primarily serves as an electricity input source into the system, with less integration into the other components. Therefore, future research should focus on better coupling PV power, wind energy, and carbon capture equipment to develop a more integrated low-carbon energy system.

4.6. Analysis of the Scheduling Model Based on IGDT

The analyses provided above are based on the assumption of certain wind power output and user load. This paper employs IGDT to study the operational outcomes of the system under uncertainties in wind power output and user load, considering two operational strategies: risk-seeking and risk-averse.

In the optimization of dispatch, the objective is to minimize system deviations under different strategies and ensure system stability. Therefore, the small differences between risk-averse and risk-seeking strategies do not indicate that the model is ineffective; rather, they demonstrate that the optimization of dispatch strategies is highly effective, especially when actual load fluctuations are minimal. The impact of these strategies is effectively controlled under conditions of low uncertainty, particularly during periods of stable wind power generation. However, if faced with larger load fluctuations or higher uncertainty, the differences between these strategies may become more pronounced.

Table 6 presents the operating costs and corresponding uncertainties under the two operational strategies in Scenario 3. Taking an opportunity deviation factor and a robustness level factor of 0.03 as an example, the value of χ changes with the operational strategy of the system.

Table 6. System operating costs under the IGDT strategy.

	χ	ε_m	δ_m	**Total Cost/Ten Thousand Yuan**
Risk-Seeking	0	0	0	180.52
	0.016	0.01	0.01	175.41
	0.106	0.03	0.03	169.48
	0.194	0.05	0.05	1624
Risk-Averse	0	0	0	180.52
	0.036	0.01	0.01	186.96
	0.075	0.03	0.03	1921
	0.104	0.05	0.05	197.87

The opportunity bias factor of 0.03 indicates that in the dispatch optimization process, we assume that the forecasted wind power generation may be 3% higher than the actual output. This assumption allows us to simulate forecast errors and evaluate their impact on grid dispatch and system operation.

The robustness factor of 0.03 reflects the system's ability to remain stable even if the actual wind power output is 3% lower than the forecasted value.

Although Figure 6 presents wind power generation data under ideal conditions with 100% forecasting accuracy, in the actual optimization process, we incorporate the opportunity bias factor and robustness factor to simulate the deviation between the forecast and actual output. This enables us to assess the system's robustness under uncertain wind conditions. Therefore, the wind power forecast in this study is not assumed to be entirely deterministic. Instead, the IGDT optimization strategy effectively captures potential discrepancies between the forecasted and actual wind power output, providing more resilient dispatch solutions to handle uncertainty.

When the system opts for a risk-seeking operational strategy, the fluctuation degree of uncertainty factors is 0.106, and the total cost at this point is 1.6948 million yuan, which is a 6.12% decrease compared to the total cost under certainty. When the system chooses a risk-averse operational strategy, the fluctuation degree of uncertainty factors is 0.075, and the total cost at this point is 19.21 million yuan, representing a 7.58% increase compared to the total cost under certainty.

Figures 11 and 12 illustrate the net power generation of the carbon capture device and the total carbon emissions of the system when both the opportunity deviation factor and robustness level are set to 0.03. The data show that under a risk-seeking strategy, the carbon capture device's net generation is lower during off-peak periods, and the system's total carbon emissions are also lower compared to the other two operating modes. In contrast, during peak load periods, a risk-averse approach leads to higher net generation from the carbon capture device and an increase in system carbon emissions.

These results indicate that while a risk-averse strategy enhances system security and robustness in response to uncertainties, it also reduces the flexibility of the carbon capture device's scheduling, impacting CO_2 processing, storage, and trading. This ultimately raises the overall system costs. On the other hand, adopting a risk-seeking strategy allows for a better utilization of uncertainties in renewable energy output and load, increasing operational flexibility and lowering costs. However, a risk-averse strategy mitigates the risks posed by uncertainties, safeguarding system safety and robustness, albeit at the expense of increased costs and reduced flexibility. Thus, for a low-carbon integrated energy system, a risk-seeking approach maximizes operational flexibility and minimizes costs, while a risk-averse strategy prioritizes stability and resilience at the cost of higher expenses.

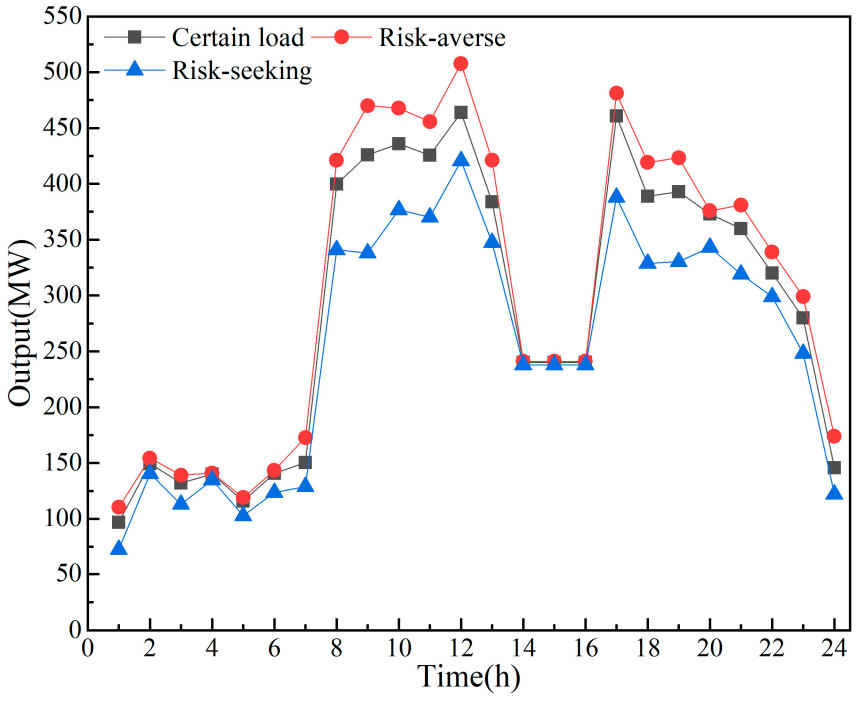


Figure 11. Net generation power of the carbon capture unit.

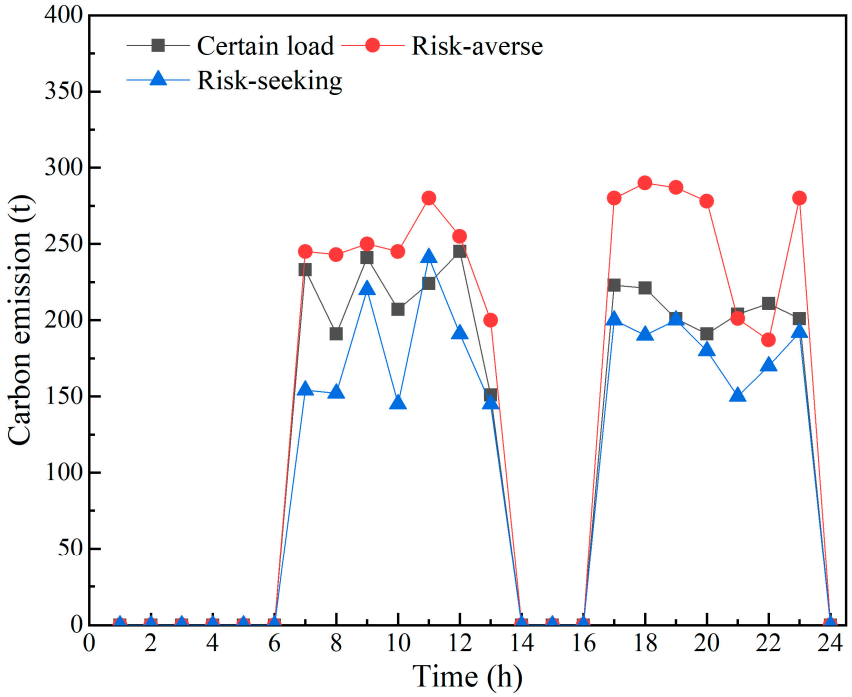


Figure 12. Total carbon emissions of the system.

5. Policy Recommendations

Despite significant technological progress in promoting the large-scale implementation of carbon capture and integrated energy systems, several key challenges remain unresolved. This section provides a brief overview of three major issues: the challenges of large-scale methanation, securing stable funding, and retrofitting carbon capture systems. Analyzing these scientific challenges and exploring potential solutions will help pave the way for the large-scale deployment of this technology and contribute to the development of low-carbon energy systems.

(1) Challenges of Large-Scale Methanation

One of the critical challenges in the methanation process is ensuring stability and efficiency in large-scale production. Although the methanation reaction (CO_2 and H_2 producing CH_4 and H_2O) has been validated in laboratories and small-scale industrial installations, several issues persist in large-scale operations.

Stringent reaction conditions: Methanation requires high temperatures and pressures, and effective heat management is crucial. In large-scale systems, maintaining control over reaction temperature and pressure to ensure sustained stability remains an unsolved problem.

Catalyst lifespan and regeneration: Catalysts in the methanation process tend to lose effectiveness over time. Extending catalyst life and reducing regeneration costs are major bottlenecks in large-scale applications.

Efficiency and economic feasibility: While methanation effectively consumes hydrogen and converts CO_2 into usable methane, improving the overall energy efficiency of the reaction, minimizing energy losses, and ensuring economic viability are scientific challenges that require further research.

(2) Funding Issues

Another significant barrier to the large-scale deployment of carbon capture and methanation technologies is funding. Particularly in developing countries like China, CCS (Carbon Capture and Storage) projects require substantial investment, covering equipment installation, operational costs, maintenance, and infrastructure development.

Long-term funding stability: Large-scale CCS projects often depend on government policy support, investments from state-owned enterprises, carbon market mechanisms, and

international cooperation. However, these funding sources are subject to uncertainty, especially due to fluctuations in the carbon market, which can impact the economic feasibility of projects. Establishing long-term stable funding sources is a critical challenge that needs to be addressed.

Policy incentives and subsidy mechanisms: While the Chinese government has introduced a range of policies to support carbon neutrality goals, there is still a lack of sufficient subsidies and incentives for large-scale CCS and methanation technology implementation. Further policy improvements are needed to encourage private sector and international investment to drive the widespread adoption of these technologies.

(3) Challenges in Retrofitting Carbon Capture Systems

Retrofitting existing coal-fired or gas-fired power plants with carbon capture systems presents numerous engineering challenges, particularly when installing carbon capture equipment on facilities that were not originally designed for it.

Space and layout issues: Many existing coal and gas plants lack sufficient space for carbon capture equipment. Finding ways to install these systems without significantly altering the existing facility layout is a major engineering challenge. Given the large size of carbon capture devices, optimizing their placement, piping routes, and system integration to avoid disrupting existing power generation processes remains a problem to be solved.

Efficiency reduction and increased operating costs: Carbon capture systems typically increase power plant energy consumption, leading to reduced overall generation efficiency. Additionally, they incur extra operational and maintenance costs. Future research should focus on developing carbon capture technologies that are more energy-efficient and stable while reducing the overall cost of application.

In this study, Ningxia, a unique province in China, was selected for the case study analysis. Located deep within China's interior and featuring vast deserts and mountainous regions, Ningxia offers geographically advantageous conditions for the investment in and operation of wind power plants. As a result, the case study optimization used data based on deterministic conditions and optimistic weather scenarios, without placing significant emphasis on investment budgets or wind resource variability. Consequently, the results inherently carry a degree of optimism, and there may be certain barriers to wider application in the future.

However, the reason for continuing this study is that Ningxia is not an isolated or unique province in China. Its natural environment is quite similar to the northwest region of China, which accounts for one-third of the country's land area. Additionally, like other provinces, Ningxia benefits from unified government investment in the construction of integrated energy systems, where profitability is not the primary concern. Therefore, although the carbon capture and hydrogen integrated energy system proposed in this paper may not be fully applicable to other countries, it holds significant reference value for the investment in and construction of integrated energy systems in China, particularly in the northwest region. This is a key objective of this study.

In summary, large-scale methanation challenges, funding sources, and retrofitting existing carbon capture systems are the main obstacles to the widespread implementation of this technological solution. Addressing these challenges will require increased research efforts and policy support to drive technological advancements and provide a solid foundation for large-scale deployment in the future.

6. Conclusions

This paper presents a system architecture for a low-carbon integrated energy system on the power generation side, considering the joint flexible operation of two-stage electrolytic hydrogen production equipment and carbon capture power plants. It constructs a comprehensive flexible operation model for carbon capture power plants and a joint operation model for two-stage hydrogen production, significantly reducing carbon emissions and operating costs of the integrated energy system on the power generation side. Moreover, it employs the IGDT algorithm to study the impact of uncertainties on system

scheduling, ensuring low-carbon, safe, and reliable operation of the system. The case study analysis leads to the following conclusions:

(1) Carbon capture power plants, considering a comprehensive flexible operation mode by integrating liquid storage tanks into the existing bypass-style carbon capture equipment, fully utilize the "energy time shift" characteristic of the storage tanks. This significantly improves the energy scheduling range of carbon capture power plants, reduces system carbon emissions, and enhances the dispatch flexibility of the low-carbon integrated energy system on the power generation side during peak and valley load periods.

(2) Two-stage P2G devices, by refining the hydrogen production and methane utilization steps in the electrolytic hydrogen production process, improve the overall energy efficiency of the system and help increase the absorption of wind energy. Additionally, by sharing electrical and thermal energy demands through hydrogen fuel cells, they reduce the energy transmission steps, further decreasing carbon emissions.

(3) The carbon capture power plant scheduling model based on IGDT theory quantitatively studies uncertainties from both risk-averse and risk-seeking perspectives. The system can choose different operational strategies based on various real-world uncertainties and safety operation requirements by selecting different opportunity deviation factors and robustness level factors.

Future research should further explore the large-scale implementation of the relevant technologies, focusing on unresolved challenges in the methanation process, long-term funding solutions, and the retrofitting of carbon capture equipment. This study addresses global sustainability challenges and seeks to explore scientific and technological solutions. By continuously optimizing energy technologies, it aims to promote the widespread adoption of clean energy systems and contribute to achieving global carbon neutrality and climate goals.

Author Contributions: Conceptualization, A.L. and M.Q.; methodology, A.L.; software, M.Q.; validation, A.L.; formal analysis, D.L.; investigation, A.L.; resources, J.Z.; data curation, A.L.; writing—original draft preparation, A.L.; writing—review and editing, A.L.; visualization, M.Q.; supervision, D.L.; project administration, J.Z.; funding acquisition, J.Z. All authors have read and agreed to the published version of the manuscript.

Funding: This research was funded by The Science and Technology Project of State Grid Corporation of China (Grant No. 5400-202218162A-1-1-ZN) and The Key Program of National Natural Science Foundation of China (Grant No. 51936003). The APC was funded by Jianguo Zhou.

Data Availability Statement: The data presented in this study are available on request from the corresponding author.

Conflicts of Interest: Author Minglei Qin was employed by the company Nanjing Power Supply Company, State Jiangsu Electric Power Co., Ltd. The remaining authors declare that the research was conducted in the absence of any commercial or financial relationships that could be construed as a potential conflict of interest.

References

1. Lu, Q.; Fang, H.; Hou, J. The impact of energy supply side on the diffusion of low-carbon transformation on energy demand side under low-carbon policies in China. *Energy* **2024**, *307*, 132817. [CrossRef]
2. Zhao, Y.; Wang, S.; Gao, G.; Xue, X.; Song, H.; Zhang, R. Exploring the green and low-carbon development pathway for an energy-intensive industrial park in China. *J. Clean. Prod.* **2024**, *459*, 142384. [CrossRef]
3. Yu, F.; Zheng, S.; Zheng, S.; Guo, C. Does carbon ETS affect the distribution of labor's slice of the factor income pie? From the low carbon transition perspective. *Energy Econ.* **2024**, *134*, 107569. [CrossRef]
4. Zeng, B.; Zhou, Y.; Xu, X.; Cai, D. Bi-level planning approach for incorporating the demand-side flexibility of cloud data centers under electricity-carbon markets. *Appl. Energy* **2024**, *357*, 122406. [CrossRef]
5. Jiang, Y.; Ren, Z.; Lu, C.; Li, H.; Yang, Z. A region-based low-carbon operation analysis method for integrated electricity-hydrogen-gas systems. *Appl. Energy* **2024**, *355*, 122230. [CrossRef]

6. Zhang, X.; Wang, X.; Tang, C.; Lv, T.; Peng, S.; Wang, Z.; Meng, B. China's cross-regional carbon emission spillover effects of urbanization and industrial shifting. *J. Clean. Prod.* **2024**, *439*, 140854. [CrossRef]
7. Wu, Y.; Aziz, S.M.; Haque, M.H. Vehicle-to-home operation and multi-location charging of electric vehicles for energy cost optimisation of households with photovoltaic system and battery energy storage. *Renew. Energy* **2024**, *221*, 119729. [CrossRef]
8. Suanpang, P.; Jamjuntr, P. Optimal Electric Vehicle Battery Management Using Q-learning for Sustainability. *Sustainability* **2024**, *16*, 7180. [CrossRef]
9. Liu, C.; Moon, D.; Watabe, A. Assessing the Economic and Environmental Impacts of Anaerobic Digestion for Municipal Organic Waste: A Case Study of Minamisanriku Town, Japan. *Sustainability* **2024**, *16*, 6793. [CrossRef]
10. Deng, Z.; Hao, Y. Energy price uncertainty, environmental policy, and firm investment: A dynamic modeling approach. *Energy Econ.* **2024**, *130*, 107306. [CrossRef]
11. Chang, Q.; Huang, Y.; Liu, K.; Xu, X.; Zhao, Y.; Pan, S. Optimization Control Strategies and Evaluation Metrics of Cooling Systems in Data Centers: A Review. *Sustainability* **2024**, *16*, 7222. [CrossRef]
12. Chen, H.; Wang, Y.; Li, J.; Xu, G.; Lei, J.; Liu, T. Thermodynamic analysis and economic assessment of an improved geothermal power system integrated with a biomass-fired cogeneration plant. *Energy* **2022**, *240*, 122477. [CrossRef]
13. Cao, Y.; Meng, Y.; Zhang, Z.; Yang, Q.; Li, Y.; Liu, C.; Ba, S. Life cycle environmental analysis of offshore wind power: A case study of the large-scale offshore wind farm in China. *Renew. Sustain. Energy Rev.* **2024**, *196*, 114351. [CrossRef]
14. Yi, T.; Zhang, C. Scheduling optimization of a wind power-containing power system considering the integrated and flexible carbon capture power plant and P2G equipment under demand response and reward and punishment ladder-type carbon trading. *Int. J. Greenh. Gas Control* **2023**, *128*, 103955. [CrossRef]
15. Xia, W.; Ren, Z.; Qin, H.; Li, H.; Yang, Z. Multinetwork constrained planning of hydrogen-power supplying facilities under double-layer coupling mechanisms. *Int. J. Hydrog. Energy* **2024**, *71*, 718–729. [CrossRef]
16. Alam, K.S.; Kaif, A.D.; Das, S.K. A blockchain-based optimal peer-to-peer energy trading framework for decentralized energy management with in a virtual power plant: Lab scale studies and large scale proposal. *Appl. Energy* **2024**, *365*, 123243. [CrossRef]
17. Song, J.; Zhang, Z.; Mu, Y.; Wang, X.; Chen, H.; Pan, Q.; Li, Y. Enhancing envrionmental sustainability via interval optimization for low-carbon economic dispatch in renewable energy power systems: Leveraging the flexible cooperation of wind energy and carbon capture power plants. *J. Clean. Prod.* **2024**, *442*, 140937. [CrossRef]
18. Li, H.; Sun, D.; Li, B.; Wang, X.; Zhao, Y.; Wei, M.; Dang, X. Collaborative optimization of VRB-PS hybrid energy storage system for large-scale wind power grid integration. *Energy* **2023**, *265*, 126292. [CrossRef]
19. Zhang, Y.; Zhao, X.; Wang, X.; Li, A.; Wu, X. Multi-objective optimization design of a grid-connected hybrid hydro-photovoltaic system considering power transmission capacity. *Energy* **2023**, *284*, 128683. [CrossRef]
20. Limb, B.J.; Markey, E.; Vercellino, R.; Garland, S.; Pisciotta, M.; Psarras, P.; Herber, D.R.; Bandhauer, T.; Quinn, J.C. Economic viability of using thermal energy storage for flexible carbon capture on natural gas power plants. *J. Energy Storage* **2022**, *55*, 105836. [CrossRef]
21. Gao, J.; Wu, H.; Gao, F. Nearly-zero carbon optimal operation model of hybrid renewable power stations comprising multiple energy storage systems using the improved CSO algorithm. *J. Energy Storage* **2024**, *79*, 110158. [CrossRef]
22. Gharun, M.; Possell, M.; Bell, T.L.; Adams, M.A. Optimisation of fuel reduction burning regimes for carbon, water and vegetation outcomes. *J. Environ. Manage.* **2017**, *203*, 157–170. [CrossRef] [PubMed]
23. Lee, W.-S.; Kang, J.-H.; Lee, J.-C.; Lee, C.-H. Enhancement of energy efficiency by exhaust gas recirculation with oxygen-rich combustion in a natural gas combined cycle with a carbon capture process. *Energy* **2020**, *200*, 117586. [CrossRef]
24. Khose, R.V.; Pethsangave, D.A.; Wadekar, P.H.; Ray, A.K.; Some, S. Novel approach towards the synthesis of carbon-based transparent highly effective flame retardant. *Carbon* **2018**, *139*, 205–209. [CrossRef]
25. Liu, B. Optimal scheduling of combined cooling, heating, and power system-based microgrid coupled with carbon capture storage system. *J. Energy Storage* **2023**, *61*, 106746. [CrossRef]
26. Mikulčić, H.; Ridjan Skov, I.; Dominković, D.F.; Wan Alwi, S.R.; Manan, Z.A.; Tan, R.; Duić, N.; Hidayah Mohamad, S.N.; Wang, X. Flexible Carbon Capture and Utilization technologies in future energy systems and the utilization pathways of captured CO2. *Renew. Sustain. Energy Rev.* **2019**, *114*, 109338. [CrossRef]
27. Chen, M.; Lu, H.; Chang, X.; Liao, H. An optimization on an integrated energy system of combined heat and power, carbon capture system and power to gas by considering flexible load. *Energy* **2023**, *273*, 127203. [CrossRef]
28. Zhu, C.; Bao, G.; Xu, R.; Song, Z.; Liu, Y. Low-carbon economic analysis of a virtual power plant with wind and solar power considering the integrated flexible operation mode of a carbon capture thermoelectric unit. *Int. J. Greenh. Gas Control* **2023**, *130*, 104011. [CrossRef]
29. Huang, W.; Luo, J.; Ge, L.; He, J.; He, Z.; Wang, X. Consider a Generalized Economic Dispatch Strategy Combining Flexible Carbon Capture Consider a Generalized Economic Dispatch Strategy Combining Flexible Carbon Capture Power Plants and Pumped Storage. *Proc. CSEE* **2024**, *44*, 1430–1445. [CrossRef]
30. Wang, Q.; Zhang, X.; Zhu, L.; Xu, D. Distributionally Robust Dispatch for Wind-Thermal-Energy Storage System with Integrated Gasification Fuel Cell-Carbon Capture Plant. *Proc. CSEE* **2023**, *1*, 1–15. [CrossRef]
31. Chaban, V.V. Exothermic barrier-free carboxylation of alkali methylates. The highest-yield synthesis of dialkyl carbonates out of alcohols and carbon dioxide rationalized and reformulated through quantum-chemical simulations. *J. Mol. Liq.* **2023**, *391*, 123244. [CrossRef]

32. Chen, Q.; Dong, Y.; Ding, J.; Wang, W.; Lu, J. Thermochemical energy storage analysis of solar driven carbon dioxide reforming of methane in SiC-foam cavity reactor. *Renew. Energy* **2024**, *224*, 120192. [CrossRef]
33. Ma, Y.; Wang, H.; Hong, F.; Yang, J.; Chen, Z.; Cui, H.; Feng, J. Modeling and optimization of combined heat and power with power-to-gas and carbon capture system in integrated energy system. *Energy* **2021**, *236*, 121392. [CrossRef]
34. Tan, Y.; Guan, L.; Huang, J.; Chen, L. A multi-stage data-driven IGDT-RO model with chance compensation for optimizing bidding of RES aggregator in competitive electricity markets. *Int. J. Electr. Power Energy Syst.* **2023**, *154*, 109396. [CrossRef]
35. Gong, X.; Li, X.; Zhong, Z. Strategic bidding of hydrogen-wind-photovoltaic energy system in integrated energy and flexible ramping markets with renewable energy uncertainty. *Int. J. Hydrog. Energy* **2024**, *80*, 1406–1423. [CrossRef]
36. Li, Y.; Wang, J.; Cao, Y. Multi-objective distributed robust cooperative optimization model of multiple integrated energy systems considering uncertainty of renewable energy and participation of electric vehicles. *Sustain. Cities Soc.* **2024**, *104*, 105308. [CrossRef]
37. van Phu, P.; Huy, T.H.B.; Park, S.; Kim, D. An IGDT approach for the multi-objective framework of integrated energy hub with renewable energy sources, hybrid energy storage systems, and biomass-to-hydrogen technology. *J. Energy Storage* **2024**, *89*, 111488. [CrossRef]
38. Yao, R.; Xie, H.; Wang, C.; Xu, X.; Du, D.; Varga, L.; Hu, Y. A multi-agent-based microgrid day-ahead optimal operation framework with liquid air energy storage by hybrid IGDT-STA. *J. Energy Storage* **2024**, *86*, 111318. [CrossRef]
39. Siqin, Z.; Niu, D.; Wang, X.; Zhen, H.; Li, M.; Wang, J. A two-stage distributionally robust optimization model for P2G-CCHP microgrid considering uncertainty and carbon emission. *Energy* **2022**, *260*, 124796. [CrossRef]
40. Liang, Y.-L.; Zhang, H.; Yang, C.-T.; Li, K.-J. Research on optimization scheduling of integrated electricity-gas system considering carbon trading and P2G operation characteristics. *Electr. Power Syst. Res.* **2023**, *225*, 109797. [CrossRef]

Disclaimer/Publisher's Note: The statements, opinions and data contained in all publications are solely those of the individual author(s) and contributor(s) and not of MDPI and/or the editor(s). MDPI and/or the editor(s) disclaim responsibility for any injury to people or property resulting from any ideas, methods, instructions or products referred to in the content.